Bloch and Wannier-Stark THz stimulated emissions in superlattices: rival of Quantum Cascade Laser?

A.A.Andronov[1], A.V. Ikonnikov[1], K.V. Maremianin[1], V.I. Pozdnjakova[1], Y.N. Nozdrin[1], A.A. Marmalyuk[2], A.A. Padalitsa[2], M.A. Ladugin[2], V.A. Belyakov[3], I.V. Ladenkov[3], A.G. Fefelov[3]

[1] Institute for Physics of Microstructures RAS, Nizhny Novgorod, Russia, andron@ipmras.ru
[2] Sigm-Plus, Moscow, Russia
[3] Federal Government Unitary Enterprise "Salut", Nizhny Novgorod, Russia

More than 40 years ago semiconductor superlattices (SLs) consisting just of simple periodic system of quantum wells (QWs) and barriers were proposed [1] as a medium with negative differential conductivity (NDC), the Bloch oscillations and high frequency lasing sources [1-3]. However all these proposals failed to provide high frequency sources due to problem of appearance of inhomogeneous electric field domains resulting from DC NDC. The domain problem was solved in quantum cascade lasers (QCLs) [4-6] by introduction SLs with complicated periods (cascade) and lasing due to injection to upper transition levels like in the first scheme in [3].

Another approach to cope with the domains was proposed in [7]: SLs with weak barriers (with low minigaps). Here at high enough electric field inter miniband tunneling provides current growth with field that prevents appearance of DC NDC and the domains formation at such fields. By using simplified quasi classical approach NDC at frequency higher than the Bloch frequency ω_B (determined by potential drop per SL period) was found in such SLs outside DC NDC [7]. Experimental studies of such SLs had found substantial role in current-voltage curve and differential conductivity of Wannier-Stark quantization in the SL under bias and had put forward possibility of the THz lasing on transition between Wannier-Stark levels (WSLs) separated several periods apart [8] (Fig. 1). The upper lasing level here is (alike in the second lasing scheme in [3]) ground WSL in SL well. The experiments [9] and the non equilibrium Green function simulations [10] demonstrate reliability of this lasing scheme.

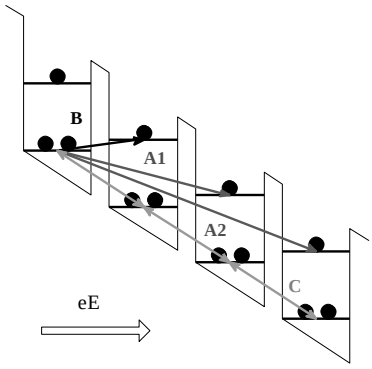

Fig. 1. Scheme of the SL portion under bias (eE) with wells and barriers shown. Relative level occupation and inter level transitions are indicated: B – absorbing; A1 and A2 – amplifying; C – Bloch transitions without direct population inversion

Here we report observation of the THz stimulated emissions from such SL (see also [11]).

The chips made of two SL wafers 1755 and 2239 (grown by MOCVD) and consist of n-type very low doped ($N \approx 4 \cdot 10^{14}$ cm^{-3}) GaAs-GaAlAs SL of 1000 periods with period d about 170 A and metal (Au) – n^+ – SL – n^+ – metal (Au) disk resonator 0.2, 0.5 and 1 mm in diameter (Fig. 2). The disc resonator was

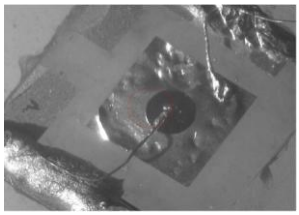

Fig. 2. Photo of the chip studied

chosen to have whispering gallery modes (WGMs) with low emission losses and dense (quasi continuum) spectrum [12], keeping in mind possible low amplification as a result of the SL low doping. The current-voltage (*I-V*) chip curve consists of ohmic part followed by DC NDC region with current oscillation (at 2–5 V), almost constant current plateau region and rising current portion due to inter miniband tunneling where the THz emissions are observed (Fig. 3).

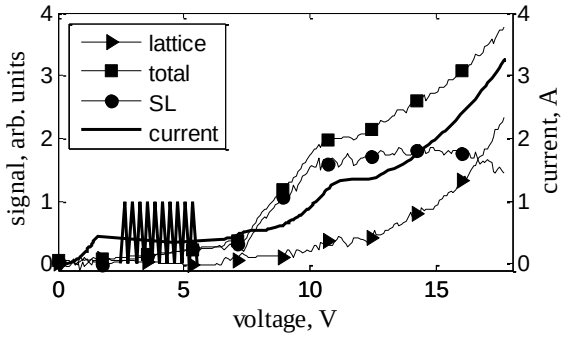

Fig. 3. Ge(Ga) detector signals and current of the 1755 SL chip

The emission observations are performed by the broad band Ge(Ga) THz detector placed in liquid helium nearby chip subject to pulsed voltage of about 10 μs in duration . The detector registers both the emission from electrons in SL and (at high voltage) also the emission due to heated chip lattice. The detector signal due to electrons in the SL shows sharp rise at about 7.5 V after the current plateau and gradual rise in current. The emission frequency bands were measured by the absorbing filter employed cyclotron resonance (CR) in the mercury-cadmium-telluride (MCT)

QW in magnetic field of superconductor solenoid placed between the chip and the Ge(Ga) detector. At voltage 8.6–10 V frequencies are higher (by about 15% – Fig. 4) of the Bloch frequency ω_B while at 12–18 V are lower ω_B. The former could be explained by the dynamic THz NDC due to tunneling to upper miniband [7] with some the NDC enhancement by WSLs transitions. The emissions at 2.8 THz at 12.8–18.8 V we consider to be due to inverted WSLs transitions [3,7,8]. By using the longer voltage pulses (up to 500 μs) chip heating above 78 K was found (by comparing end pulse current with the one at 78 K and higher temperatures measured at short pulses) with eventually no change of detector signal produces by electrons in the SL. This points to prospect for elevated temperature and CW operation.

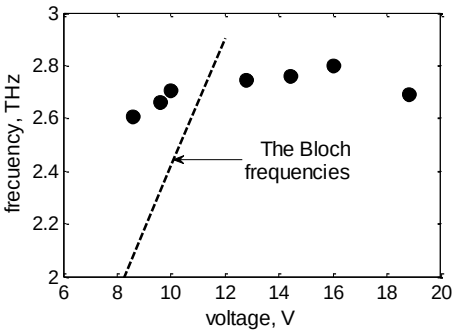

Fig. 4. Emission frequencies versus voltage

The lasing nature of the emissions is supported by the Ge(Ga) detector signal sharp rise at about 7.5 V and narrow emission lines which are only a little bit higher than the line of a THz QCL measured in the same approach. Also the CR absorption dips for 8–10 V (where contribution by lattice emission is small) are about that of the QCL pointing to absence substantial emission frequencies outside frequency of the CR dip here. At higher voltages lattice emission (measured with strobe out of end of voltage pulse) appears (Fig. 3). The CR absorption dip decreases but its width does not change pointing to survival of the narrow band of the SL emission with temperatures rise.

Anyway the results are the first demonstration of the THz amplification in simple SL outside DC NDC region. The SL studied is by no means optimal to produce the THz stimulated emission: it has very low doping and not low the Joule losses. Still the results strongly support the stimulated nature of the emission observed and their existence at T >100 K. So the authors can well claim that the proposed route [8-10] is quite promising for creation of the THz and higher frequency sources based on such simple SLs. Such sources based on weak barrier GaAS-GaAlAs SLs with SLs and chips parameter optimization should well compete with the THz QCLs especially at elevated temperatures. The optimization must include higher SL doping (up to $N \approx 1–5\cdot10^{15}$ cm^{-3})), lower thicknesses of n+ contact layers (to about 0.1 μm). Already these changes should permit to decrease two-three times number of SL periods needed for the lasing. Also optimization (decreasing) of the SL barrier strength should provide increase in amplification: calculations show that the strength decrease increases the inter W.-S. transition matrix element [9] (supplementary material) while the Green function simulations [10] directly demonstrate some amplification increase. Change of the emission frequency can be achieved by change in SL period with appropriate change in barrier strength: higher frequencies need shorter period, higher barrier strength and higher applied fields. The shorter period SLs should be less sensitive to possible suppression [10] of two-three period tunneling by increased doping. Other material system could be promising for the THz SL sources studied. In particular the THz sources based on simple weak barrier SLs made of GaN-AlGaN heterostructures look excitingly promising for the THz sources with high temperature operation (presumably up to room temperature) due to a very high polar optical phonon energy (nearby 1000 K). This heterostructure system was used recently for creation of 5–7 THz QCLs [13].

References

1. *Esaki, L., Tsu, R.* Superlattices and Negative Differential Conductivity in Semiconductors // IBM Jour. Res.Dev. 1970. V. 14. P. 61–65.

2. *Ktitorov, S. A., Simin, G. S., Sandolovski, V. Ya.* Bragg reflection and the high-frequency conductivity of electronic solid-state plasma // Sov.Phys.-Solid State 1971. V. 13. No. 8. P. 1872–1874.

3. *Kazarinov, R. F., Suris, R. A.* Possibility of amplification of electromagnetic waves in a semiconductor with superlattice // Sov.Phys.Semicond. 1971. V. 5. P. 707–709.

4. *Faist, J., Capasso, F., Sivco, D. L. et al.* Quantum cascade laser // Science 1994. V. 264. P. 553–557.

5. *Kohler, R., Tredicucci, A., Beltram, F. et al.* Terahertz semiconductor-heterostructure laser // Nature 2002. V. 417. P. 156–159.

6. *Williams, B. S., Kumar, B. S., Callebaut, H., Hu, H.* Terahertz quantum cascade laser at $\lambda \approx 100$ microns using metal waveguide for mode confinement // Appl. Phys. Lett. 2003. V. 82. No. 11. P. 2124–2127.

7. *Andronov, A. A., Nefedov, I. M., Sosnin, S. V.* Transport in narrow minigap superlattices and the Terahertz Bloch oscillator // Semiconductors 2003. V. 37. No. 3. P. 378–383.

8. *Andronov, A. A., Dodin, E. P., Zinchenko, D. I. et al.* Amplification of terahertz radiation on transitions between Wannier-Stark ladders in weak-barrier superlattices // Quantum Electronics 2010. V. 40. No. 5. P. 400–405.

9. *Andronov, A. A., Dodin, E. P., Nozdrin, Yu. N. et al.* Stimulated Emission at Transitions between Wannier-Stark Ladders in Semiconductor Superlattices // JETP Leters 2015. V. 102. No. 4. P. 207–211.

10. *Winge, D. O., Frianckie, D. O., Wacker, A.* Superlattice gain in positive differential conductivity region // AIP Advances 2016. V. 6. P. 045025.

11. *Andronov, A. A., Ikonnikov, A.V., Maremianin, K.V. et al.* THz Stimulated Emission from Simple Superlattice in Positive Differential Conductivity Region // Semiconductors 2018. V. 52. No. 4. P. 431–435.

12. *Andronov, A. A., Dodin, E. P., Nozdrin, Yu. N. et al.* Modes, emission beams and losses of THz heterostructure disk lasers: single-mode laser with vertical beam option // Electronics Letters 2016. V. 52. No. 5. P. 383–385.

13. *Terashima, W. Hirayama, W.* GaN-based THz QCLs // Proceeding SPIE 9483, p. 948304.

THz Quantum Cascade Laser disc cavities emission beams and losses

A.A.Andronov, V.I. Pozdnjakova

Institute for Physics of Microstructures RAS, Nizhny Novgorod, Russia, andron@ipmras.ru

Vertical emission beams and single frequency emission produces by simple design is a common dream for producers of any heterolasers. With vertical emission it is easy to feed appropriate emission guiding system. Also with such lasers chips it is simple to produce multiple chip system on one laser wafer e.g. to increase output power. Only vertical cavity surface emitted lasers have intrinsically such properties. Also higher (second) order distributed feedback systems and their modification can provide vertical emission. But such approach required sophisticated enough fabrication process (see e.g. appropriate works on THz QCLs [1-3]). THz QCLs [4] nowadays use metal - active region - metal cavities introduced in [5]. Seems such disc cavities considered silently as inappropriate for supporting high emission vertical beam because it is thought that in disc cavity only low emissive whispering gallery modes (WGMs) propagating along disc rim should be excited. Surely in a disc there are non WGMs propagating across disc and in particular along disc diameter. It is possible to suppress competing WGM by mode selection or by introducing additional absorption at disk rim suppressing WGMs. The modes propagating along disc diameter is alike the modes in strip ridge cavity. But they are broader and take almost the whole of the disc rim and specifically for TEM_{1m} has high emission vertical beam. Discussion of the last possibilities (and related problems of these modes selection form other disc modes) is the subject of this report.

The discussion is based on magnetic current picture which is commonly used in discussion and calculation of slit and patch antennas (see e.g. [6-8]). But we know no publication where such approach was thoroughly considered and applied to find emission losses and emission diagram of THz heterostructure laser cavity (only brief discussion of such approach together with disk THz QCL experimental emission data is presented in [9]). In the report we first introduce a notion of magnetic current and its use for micro strip-line emission calculations. Then properties of disc cavities with set of diameters and design for TEM modes at wavelength 100 micrometers are discussed.

Magnetic current describes behavior of electric field at slits in a metal sheet crossed by electrical current or at rims of strip lines. In these cases distribution of electric field across slit in metal or across rim of strip line (both crossings supposed to be substantially lower than electromagnetic wavelength in free space) can be found independently. In particular for the strip lines resonator discussed it is supposed that emission losses are small (resonator modes quality factor is substantially higher than unity) and strip line modes field distributions can be found without taking into account the emission. Then basing on those distributions emission losses and diagrams are found. The emission calculations are the following. With determined electric field across strip line rims (supposing that dimension of rims – distance of metallic parts of strip lines – are substantially smaller than wavelength in free space) we neglect the rim dimension. Now one has metallic plane with slits in the plane corresponding to strip position with known electric fields across slits tangent to the plane. Such electric field distribution provides unique electromagnetic fields out of the plane (see e.g. [7, 8]). Next we exclude slits by considering intact metallic plane (plane without slits) but with introduced magnetic surface current distribution $\mathbf{j}_m^S$ tangent to the plane at rim positions according to expression similar to connection between surface electric current at metallic plane and magnetic field (see [7]): $(4\pi/c)\ \mathbf{j}_m^S = [\mathbf{n}\ \mathbf{E}]$. Here $\mathbf{n}$ is normal to the plane. By integrating electric field over rim dimension d we get concentrated surface magnetic current $\mathbf{I}_m^S = (cd/4\pi)\ [\mathbf{n}\ \mathbf{E}]$ expressed via potential drop across the rims $U = dE$. This concentrated surface magnetic current $\mathbf{I}_m^S$ should (or could) be used to calculate emission over the plane. Because of constructive interaction surface magnetic current $\mathbf{I}_m^S$ with ideal metal (i.e. mirror current is of the same direction as the primary magnetic current) the magnetic current emission in such systems can be found just from emission of double current in free with taking only emission above the plane. Scheme of magnetic currents for TEM_{12} modes providing vertical beam is presented in Fig 1. For calculation details see [9].

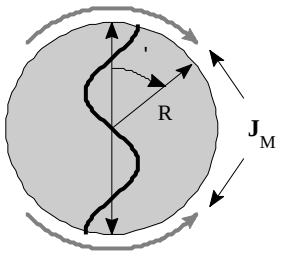

Fig. 1. Scheme of TEM_{12} mode and magnetic currents $\mathbf{J}_M$ at the disk rim for the mode which provide narrow vertical emission beam.

Fig. 2 gives examples of calculated beams and emission losses (expressed as effective mode absorption coefficient) for several disc cavities designed for 100 micron wavelength. We see what beams are directed in vertical direction and emission losses are quite high: of about or higher than amplification coefficient in standard THz QCL with 10 microns active region thickness. To overcome such situation with vertical beams more thinner active region in TH QCLs should be used alike the one in [10].

Also TEM_{1m} mode selection from WGMs should be dealt with.

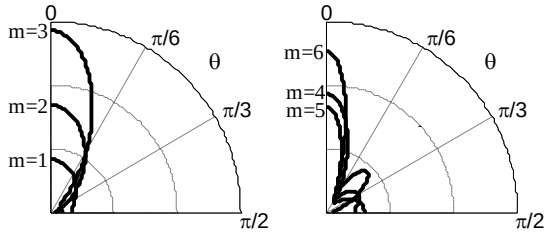

Fig. 2. Calculated beams for disk mode TEM_{1m} at λ=100 μm for disk radius 8, 23, 38, 52, 66 and 80 μm; corresponding mode effective absorption coefficients for d = 10 μm are 94, 34, 19, 30, 33 and 22 cm^{-1}

References

1. *Mahler, L., Tredicucci, A.* Photonic engineering of surface-emitting terahertz quantum cascade lasers // Laser Photonics Rev. 2011. V. 5. P. 647–658.

2. *Yu, N., Wang, G., Capasso, F.* Beam Engineering of quantum cascade lasers // Laser Photonics 2012. V. 6. No. 1. P. 24–46.

3. *Sirtori, C., Barbieri, S., Colombelli, R.* Wave engineering with THz quantum cascade lasers // Nature Photonics 2013. V. 7. P. 691–701.

4. *Kohler, R., Tredicucci, A., Beltram, F. et al.* Terahertz semiconductor-heterostructure laser // Nature 2002. V. 417. P. 156–159.

5. *Williams, B. S., Kumar, B. S., Callebaut, H., Hu, H.* Terahertz quantum cascade laser at $\lambda \approx 100$ microns using metal waveguide for mode confinement // Appl. Phys. Lett. 2003. V. 82. No. 11. P. 2124–2127.

6. *Balanis, C.A.* Antenna Theory: Analysis and Design. 3nd edition. Wiley Interscience. Chapter 14. Microstrip Antennas.

7. *Weinstein, L. A.* Electromagnetic Waves, 2nd edition. Moscow: "Radio I Svyaz" (in Russian) 1988.

8. *Jackson, J. D.* Classical Electrodynamics. Wiley. New York and London. 1962.

9. *Andronov, A. A., Dodin, E. P., Nozdrin, Yu. N. et al.* Modes, emission beams and losses of THz heterostructure disk lasers: single-mode laser with vertical beam option // Electronics Letters 2016. V. 52. No. 5. P. 383–385.

10. *Chassagneux, Y., Palomo, J., Colombelli, R. et al.* Low threshold THz QC laser with thin core regions // Electronics Letters 2007. V. 43. No. 5. P. 285–286.

Long wavelength InAs- based quantum cascade lasers

A. N. Baranov, Z. Loghmari, M. Bahriz, R. Teissier

IES, University of Montpellier, Montpellier, France, baranov@univ-montp2.fr

Quantum cascade lasers (QCL) have now become a versatile laser technology covering an extremely broad spectral range from mid-infrared to THz frequencies. These devices can be referred to as GaAs-, InP- and InAs-based QCLs depending on the substrate used for their growth (Fig. 1). The initial interest to the InAs/AlSb material system was due to the giant conduction band offset of 2.1 eV between InAs and AlSb, which made it possible to obtain high energies of intersubband transitions and to demonstrate the shortest QCL emission wavelength of 2.6 µm [1]. The small electron effective mass in InAs is another property of antimonides attractive for use in QCLs, which can provide a higher intersubband gain compared with other materials. This advantage can be fully exploited in long wavelength devices emitting beyond 10 µm, where the active quantum levels of the laser transition are close to the bottom of the conduction band and the electron effective mass is not increased by the nonparabolicity effects. Even the first long wavelength mid-infrared InAs-based QCLs outperformed InP- and GaAs-based counterparts operating in the 16–24 µm. With these QCLs we demonstrated the first semiconductor lasers operating at room temperature up to a wavelength of 21 µm.

Important progress in the device performances has been achieved through use of a dielectric waveguide instead of a usually employed in far infrared QCLs double metal surface plasmon waveguide. Doped InAs cladding layers provide optical confinement in such a waveguide. The waveguide improvement was then completed with a design and doping optimization, which resulted in demonstration of the first room temperature continuous wave (cw) operation of InAs-based QCLs achieved at 15 µm [2]. Recently we obtained RT cw operation of QCLs emitting at 17.8 µm thus establishing a new record for semiconductor lasers (Fig.2). We have also demonstrated a maximum temperature of cw operation of 320 K for QCLs emitting near 11µm [3] and 240 K at 21 µm. InAs-based QCLs operating between 11 and 20 µm exhibit pulsed threshold current density in the range 0.6-1 kA/cm^2 at RT.

Multiphonon absorption is a fundamental problem limiting performances of mid-infrared QCLs emitting below the reststrahlen band. This mechanism made impossible to obtain lasing from InP-based QCLs emitting near 16 µm [4]. The multiphonon absorption bands of different materials do not coincide, which gives a possibility of full coverage of the mid-infrared range close to the reststrahlen band. In particular, we demonstrated high performance InAs-based QCls operating in the cw regime in the spectral region around 16 µm, prohibited for the InP-based devices. On the other hand, the two-phonon absorption in InAs near 23 and 27-29 µm makes difficult to obtain lasing from InAs/AlSb QCLs in the vicinity of these wavelengths. The longest emission wavelengths of the InAs/AlSb lasers are located around 25 µm [5], whereas InP-based QCLs emitting at 28 µm were successfully demonstrated. In these devices InAlAs barriers in the active zone were replaced by GaSbAs in order to avoid fundamental AlAs-like phonon absorption. Taking also into account the fundamental phonon absorption in AlSb between 29 and 32 µm one can conclude that to move farther into the far-infrared with InAs/AlSb QCLs it is necessary to target wavelengths above 34 µm. Fabrication of QCLs operating in this spectral range will be a difficult task because of other limitations, such as strong free

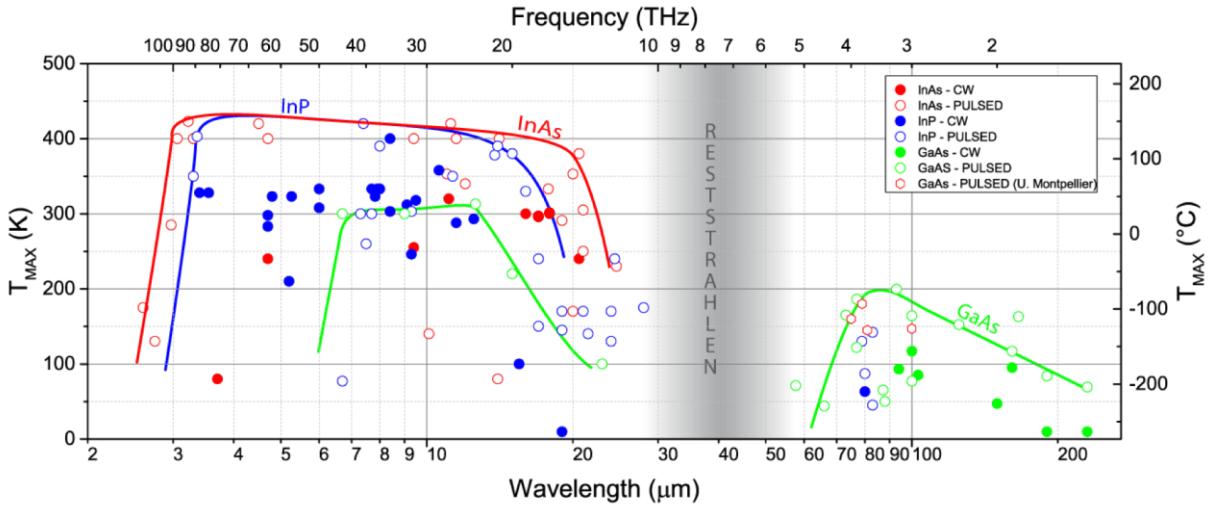

Fig. 1. Maximum operation temperature of quantum cascade lasers: state of the art.

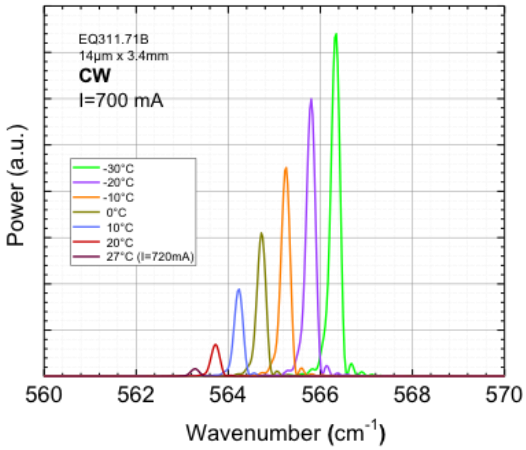

Fig.2. Emission spectra of an InAs/AlSb DFB QCL in the continuous wave regime at different temperatures. Single frequency cw regime is achieved at 17.8 µm at 300K.

carrier absorption and the small difference between the transition energy and the energy of the LO-phonon in InAs.

The small electron effective mass in InAs can also be helpful to obtain high intersubband gain in QCLs operating in the THz domain and thus to increase their operation temperature but no lasing has not yet been obtained.

References

1. *Cathabard, O. at al.* Quantum cascade lasers emitting near 2.6 µm // Appl. Phys. Lett. 2009, V. 96, P. 111118-1-111118-3.

2. *Baranov, A.N., Bahriz, M., Teissier,R.,* Room temperature continuous wave operation of InAs-based quantum cascade lasers at 15 µm.// Optics Express 2016, V. 24, P. 18799.

3. *Loghmari, Z., Bahriz, M., Díaz Thomas, D., Meguekam, A., Nguyen Van, H., Teissier, R., Baranov, A.N.,* Room temperature continuous wave operation of InAs/AlSb-based quantum cascade laser at 11 µm// Electronics Letters 2018, V. 54, P. 1045-1047.

4. *Rochat, M., Hofstetter, D., Beck, M., Faist, J.,* Long-wavelength (λ≈ 16 µm), room-temperature, single frequency quantum-cascade lasers based on a bound-to-continuum transition // Appl. Phys. Lett. 2009, V. 79, P. 4271-4273.

5. *Loghmari, Z., Bahriz, M., Teissier, R., Baranov, A.N.,* InAs-based quantum cascade lasers emitting close to 25 µm // submitted to Electronics Letters 2018.

Metrological Grade THz Radiation

Luigi Consolino[1], M. De Regis[1], F. Cappelli[1], S. Bartalini[1], P. De Natale[1]

[1]INO, Istituto Nazionale di Ottica-CNR, Largo E. Fermi, 6 Firenze I-20125, Italy
luigi.consolino@ino.it

In the last few decades, the THz window of the electromagnetic spectrum has emerged as enabling breakthrough scientific and technological applications in such diverse fields as information and communications technology (ICT), biomedicine, homeland security, quality control of food and global environmental monitoring. Likewise, high precision THz spectroscopy of rotational and ro-vibrational molecular transitions promises to deliver many novel physical insights. Two different approaches for THz metrological-grade radiation will be presented, the first related to optical frequency comb (FC) based broadband continuous wave (CW) THz source, the second regarding the generation, characterization and possible applications of Quantum Cascade Lasers (QCL) based THz FCs.

1. FC-based broadband CW THz source

Regarding THz frequency metrology, a lot of work as been done on single mode QCL setups [1]. However, in order to fully exploit the potential of this key spectral region, the challenge is to merge, in a single source, three crucial aspects: an even broader spectral coverage towards higher THz frequencies (covered neither by QCLs nor by other traditional THz sources), metrological-grade performances (i.e. high resolution and accuracy with referencing to the primary frequency standard), power levels sufficient for room-temperature detection.

In our work we demonstrate room-temperature generation and detection of continuous-wave THz radiation spanning three octaves in the THz range, from 1 to 7.5 THz, and performing high-accuracy molecular spectroscopy. This unprecedented result builds on attempts that have lasted for more than 30 years (for a recent review see [2]), and makes use of a simple, reliable approach that combines, in a unique set-up, robust telecom laser components with difference-frequency nonlinear generation.

In synthesis, the main contribution of our work is the combination of all the following aspects: i) room temperature CW generation, based on the fully-developed and commercial telecom fiber laser technology that grants a high level of compactness, stability and reliability to our new source; ii) a 3-octave spectral coverage, from 0.97 to 7.5 THz, that is obtained by the combined use of a Cherenkov emission scheme and strong light confinement in a surface nonlinear waveguide; iii) high power levels enabling both room temperature detection and high-precision THz spectroscopy, achieved thanks to a CW generation efficiency as high as 10^{-7} W^{-1} ; iv) frequency referencing to the primary frequency standard by means of a mode-locked femtosecond laser and a GPS disciplined Rubidium-Quartz oscillator; v) a state-of-the-art accuracy in the order of 10^{-9} obtained with a room temperature Golay cell detector.

Fig. 1 shows the spectroscopic potential of our source, applied to low pressure methanol gas vapors, going from a 40 GHz span to Doppler limited absorption profiles.

The proposed approach paves the way to a new class of metrological-grade sources spanning most of the THz range for countless demanding applications.

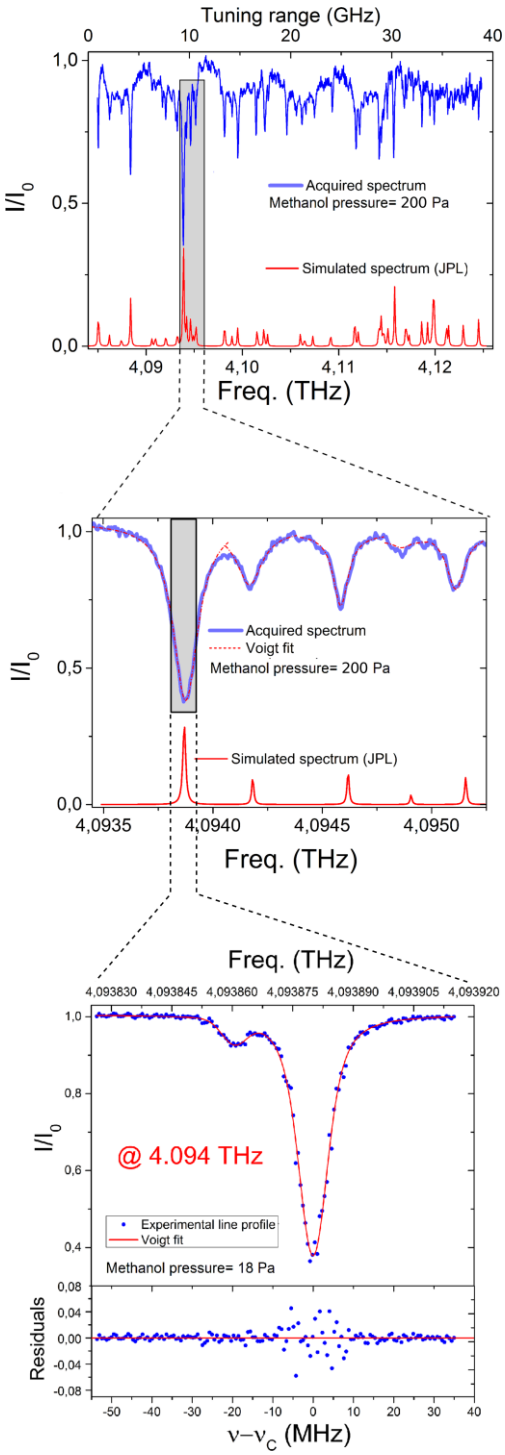

Fig. 1. Precision spectroscopy on low pressure methanol vapours, and comparison to molecular database.

2. Free-standing THz frequency combs

The invention of Optical Frequency Combs (FCs) by Prof. Theodor Haensch (Nobel Prize 2005) and co-workers has represented a major improvement, if not a vast revolution, in the field of frequency metrology. The most common sources for FCS are mode-locked lasers, whose high level of coherence enabled a myriad of scientific applications, providing a frequency ruler for any laser emitting within their spectral range. For this reason huge efforts have been spent to extend the characteristics of FCSs to all spectral regions, and to extend the figure of merits of FCSs to other non-conventional comb-like source.

In this framework Quantum Cascade Lasers (QCLs) technology, both in the mid-infrared and THz region, is exploiting the extraordinary versatility of these sources for developing active regions with engineered optical dispersion that emit optical frequency combs (OFC). There are a lot of similarities with ultrashort-pulse lasers, such as the constant spacing between modes, that is defined by the cavity length, and that results in a very narrow and stable "intermodal beatnote". Other evidence that multimode THz QCL sources behave as frequency combs (QCL-combs) has already been provided [3,4]. However, the strongest signature of comb operation, that is the demonstration of a constant phase relation simultaneously measured among the emitting modes, is still missing.

Here we present a general experimental approach capable of simultaneously measuring the phase relations among the modes of a comb source, and of verifying its time evolution. We have tested the potential of our technique on commercial mode-locked near-IR lasers and we have then performed measurements on both mid-infrared and THz QCL-combs. The obtained results provide complete answers to the questions above, and give an important contribution to assess the comb operation of QCLs.

The experiment is based on the frequency-domain analysis of the time-evolving multi-heterodyne signal obtained by beating the QCL with a metrological-grade FC emitting in the same region (see fig. 2) [5].

The mode spacing of the THz QCL-combs is electronically locked to an RF reference. The obtained signal is processed in order to remove the common frequency noise contribution. The signal is acquired as time traces, then each acquisition is split into shorter consecutive frames and the Fourier transform of each frame is computed. From the generated dual comb signal it is possible to retrieve the spectrum of the QCL-comb, and to study the time evolution of each mode, in terms of amplitude, frequency and phase.

The precision of our measurement technique has been also tested by using synthesized signals, and results to be better than 0.01°. An example of the acquired data, is given in fig. 3, where the FFT phases corresponding to the peaks positions are shown for different frames. The fact that, during the acquisition time, the phases are well confined, confirms the phase coherence of the QCL comb sources, and gives an evidence of the frequency-comb nature of this new kind of coherent sources.

The possible availability of a second independent actuator for the QCL-comb parameters, that is presently under investigation, will likely enable full control of the whole emitted spectrum, allowing the narrowing of all the comb modes down to the above mentioned level.

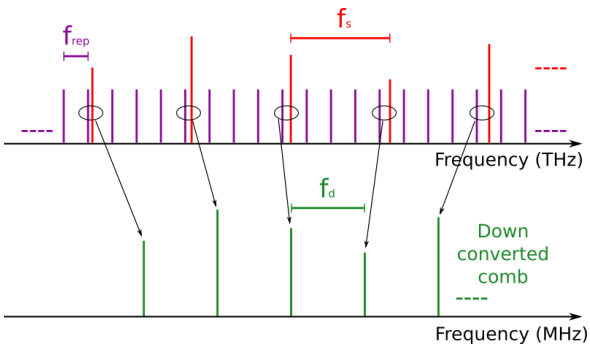

Fig. 2. Multi-heterodyne down-conversion scheme.

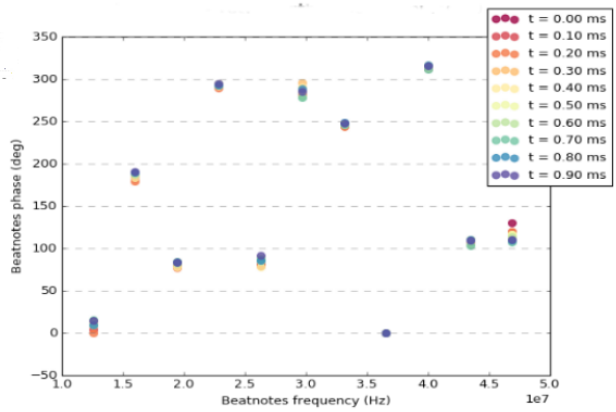

Fig. 3. Phases of the modes of a THz QCL comb experimetnally obtained by Fourier transform

References

1. *Bartalini, S., Consolino, L., Cancio, P., et al.* Frequency-comb-assisted THz quantum cascade laser spectroscopy // Phys. Rev. X 2014 V. 4, P. 021006.

2. *Consolino, L., Bartalini, S., De Natale, P.* Terahertz frequency metrology for spectroscopic applications: a review // J. Infrared Milli Terahz Waves, 2017 V. 38, No. 11, P. 1289–1315.

3. *Burghoff, D., Kao, T.-Y., Han, N., et al.* Terahertz laser frequency combs // Nat. Photonics 2014 V. 8, P. 462–467.

4. *Burghoff, D., Yang, Y., Hayton, D.J., et al.* Evaluating the coherence and time-domain profile of quantum cascade laser frequency combs // Opt. Express 2015 V. 23, P. 1190.

5. *Consolino, L., Taschin, A., Bartolini, P., et al.* Phase-locking to a free-space terahertz comb for metrological-grade terahertz lasers // Nature Commun. 2012 V. 3, P. 1040.

Investigation of the emission spectra of pulsed THz quantum cascade lasers and their use for magnetospectroscopy of semiconductors

K.V. Maremyanin[1], A.V. Ikonnikov[2], V.I. Gavrilenko[1], N.N. Mikhailov[3], S.A. Dvoretskii[3]

[1]Institute for Physics of Microstructures Russian Academy of Sciences, Nizhniy Novgorod, Russia, kirillm@ipmras.ru
[2]Lomonosov Moscow State University, Faculty of Physics, Moscow, Russia
[3]Rzhanov Institute of Semiconductor Physics, Siberian Branch of RAS, Novosibirsk, Russia

Quantum cascade lasers (QCL) are compact solid-state sources operating both in mid-IR and THz frequency ranges [1]. The paper is devoted to investigation into possibility of THz QCL frequency tuning and gives an example for their application for magnetospectroscopy of semiconductor nanostructures.

THz QCLs under study were manufactured by “Trion Technology” (Tempe, Arizona, USA) [2,3]. The active region consisted of multilayer $GaAs/Al_{0.15}Ga_{0.85}As$ heterostructure with the design of "resonance emission of an optical phonon" placed in a double metal band waveguide 80-100 μm wide and 1–2 mm long, cavity mirrors being formed by cleaved in (110) crystallographic direction surfaces. Measurements were carried out in the pulsed mode, QCLs being mounted on a cold finger in a closed cycle cryostat (T = 7-80 K). Spectral investigations were carried out with Fourier-transform spectrometers and the signal was recorded with Ge:Ga impurity photoresistor.

Emission characteristics of QCL proved to not undergo significant changes up to 50 K, after which a noticeable decrease in the radiation intensity was observed, that results from the drop of electron lifetime at the upper working level due to the increased scattering rate of electrons by acoustic phonons. The maximum QCL operating temperature was about 80 K. Typical emission spectra of 4.3 THz QCL measured at different temperatures at one and the same injection current are given in Fig. 1.

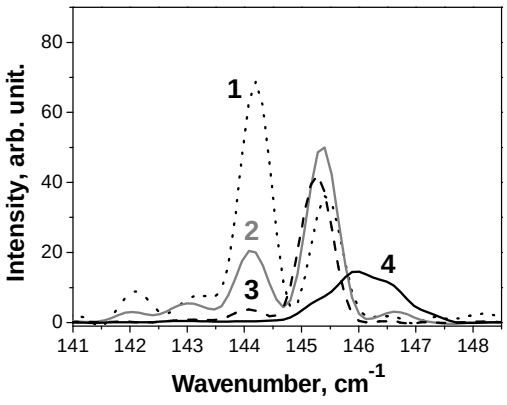

Fig. 1. QCL emission spectra in 4.3 THz range measured for one and the same current 1.4 A with the spectral resolution of 0.5 cm^{-1}. T, K: 1 – 7, 2 – 50, 3 – 70, 4 – 80 [2].

One can see two main spectral lines at frequencies near 144 cm^{-1} and 145.5 cm^{-1} corresponding to two longitudinal modes of QCL Fabry-Perot resonator. The temperature increase results in a "transfer" of intensity from the low-frequency mode to the higher-frequency low. This effect can be explained by both the decrease in the gain and the increased absorption of electromagnetic radiation by free carriers, which is proportional to the wavelength square. Together, these factors result in the maximum gain shift to higher frequencies.

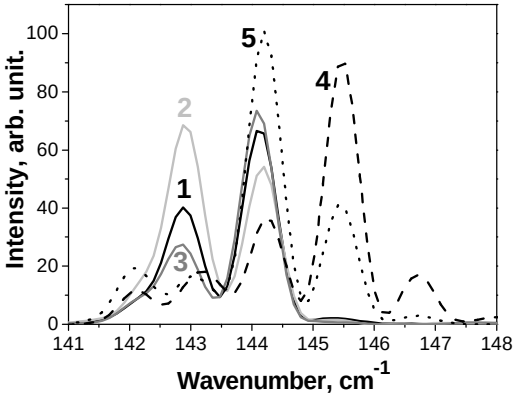

Fig. 2. Emission spectra of the 4.3 THz QCL measured at T = 7 K with the spectral resolution of 0.5 cm^{-1} at different positions (in time) of the sampling pulse (strobe) for three values of the applied voltage: 1 - 14.4 V (the entire pulse), 2 - 14.4 V (beginning of the pulse), 3 - 14.4 V (pulse end), 4 - 15.3 V (beginning of the pulse), 5 - 15.8 V (beginning of the pulse) [2]. The entire pulse duration is 10 μs.

The similar shift of the radiation intensity into higher frequency modes was discovered at the increase of the applied voltage and the time delay of the signal acquisition during QCL emission pulse 10 μs in duration - Fig. 2. Spectra 1 to 3 are obtained one and the same applied voltage of 14.4 V. The first one is averaged over the most part of the radiation pulse (that corresponds to the measurement condition in Fig. 1). For this purpose, the sampling duration (strobe) at the boxcar integrator was chosen almost equal to the duration of the radiation pulse (10 μs). Spectra were measured with the strobe duration of 30 μs, the 2-nd spectrum being obtained at the strobe positioned at initial part of the radiation pulse and the 3-rd one - at the end of the pulse. It is clearly seen that the "integral" spectrum is, in fact, a superposition of the 2-nd and the 3-rd spectra. As easy to see, during the pulse the radiation intensity is “transferred” from the low-frequency modes to the high-frequency ones that is a consequence of the QCL active region heating during the pulse of the applied voltage. An increase in the applied voltage (and the current) also leads to a similar effect. The 2-nd, 4-rth and 5-th

spectra were measured at the strobe positioned at initial part of the radiation pulse at applied voltage 14.4 V, 15.3 V and 15.8 V, respectively. It is seen that with voltage rise, the intensity of the high-frequency modes increases consecutively while the intensity of the low-frequency ones decreases, that is also most likely due to the QCL heating.

Results of high resolution (0.01 cm^{-1}, 300 MHz) spectral measurements of 3.2 THz QCL at different temperatures 10 to 60 K are given in Fig. 3. One can see that QCL emission mode is shifted to LOWER frequencies with the temperature increase from 107.00 to 106.91 cm^{-1}, that corresponds to a 2.7 GHz tuning range. The effect results from the change in QCL active region averaged refractive index. It was also shown that the mode frequency is tuned during the generation pulse, that opens a possibility to use the effect of "fine" QCL mode frequency sweeping for THz spectroscopy of gases [3].

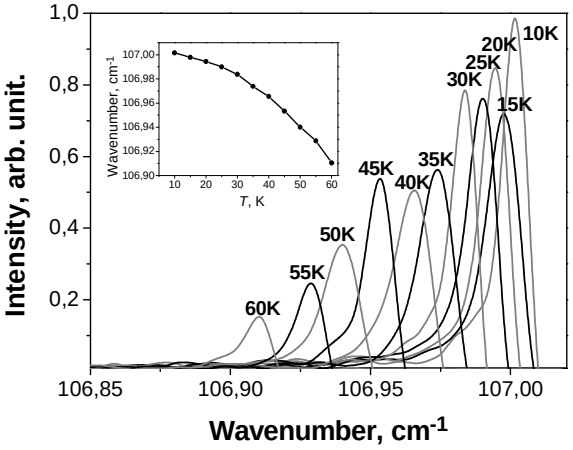

Fig. 3. Emission spectra of the 3.2 THz QCL measured at T = 10 - 60 K and applied voltage 14.8 V with high spectral resolution 0.01 cm^{-1}. The inset shows the dependence of the QCL mode frequency on the temperature [3].

To demonstrate the possibility of QCL using for the spectroscopy of semiconductors, the magnetoabsorption of $Hg_{0.843}Cd_{0.157}Te/Cd_{0.564}Hg_{0.436}Te$ quantum well (QW) heterostructure (sample #100708) was studied. The nominal thickness of the quantum well HgTe QW was 30 nm. Fig. 4 presents typical cyclotron resonance (CR) spectra of the sample #100708 at several 2D electron concentrations (varied due to persistent photoconductivity effect) measured using QCL as a radiation source. To identify the observed lines, the positions of the absorption peaks were plotted on the frequency–magnetic field plane together with the data obtained by Fourier-transform spectroscopy technique (Fig. 4, inset). As easy to see, the data obtained by different experimental techniques (open and closed symbols) are in excellent agreement with each other. Comparing the experimental data with the calculation results provides unambiguous identification of the observed transitions [4].

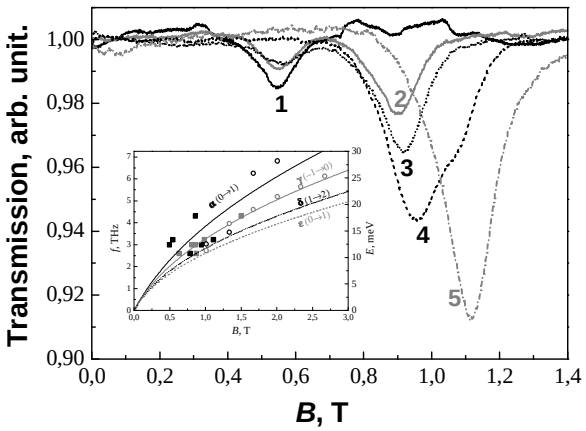

Fig. 4. Typical CR spectra of the sample #100708 obtained with QCL operating at 3.23 THz in the absence of interband illumination (1) and at various levels of illumination (2–5). 2D electron concentrations in units of 10^{10} cm^{-2} are (1) 1.8, (2) 3.1, (3) 3.7, (4) 5.4, and (5) 8.7. The inset shows the calculated magnetic field dependence of the transition energies (lines) and positions of the CR spectral lines (symbols). Open and closed symbols are the experimental results obtained with the use of the Fourier-transform spectrometer and QCL, respectively.

This work was financially supported by the Russian Foundation for Basic Research (Grant #18-52-00011). The work was done using equipment of Common Research Center "Physics and technology of micro- and nanostructures" at IPM RAS.

References

1. *Vitiello, M. S., Scalari, G., Williams, B., De Natale, P*. Quantum cascade lasers: 20 years of challenges // Opt. Express. 2015. V.23, No. 4. P. 5167-5182.

2. *Antonov, A. V., Gavrilenko, V. I., Ikonnikov, A. V.. Maremyanin, K. V., Lastovkin, A. A., Morozov, S.V., Ushakov, D. V., Sadofyev, Yu.G., Samal, N.* Emission spectra of terahertz quantum cascade laser // Radiophysics and Quantum Electronics. 2009. V. 52, No. 7. P.494-499.

3. *Lastovkin, A. A., Ikonnikov, A. V., Gavrilenko, V. I. , Antonov, A. V., Sadofyev Yu. G.* . Studying the frequency tuning of pulsed terahertz quantum cascade lasers // Radiophysics and Quantum Electronics. 2011. V. 54, No. 8-9. P.609-615.

4. *Ikonnikov A.V., Zholudev M S., Marem'yanin K.V., Spirin K.E., Lastovkin A.A., Gavrilenko V.I., Dvoretskii S.A., and Mikhailov N.N.*. Cyclotron resonance in HgTe/CdTe(013) narrowband heterostructures in quantized magnetic fields // JETP Lett. 2012. V. 95, No. 8. P. 406–410.

Reconfigurable terahertz optics based on etched structures in vanadium dioxide thin films

P. M. Solyankin[1,2,*], M. N. Esaulkov[1,3], O. E. Kameshkov[4,5], B. A. Knyazev[4,5], A. P. Shkurinov[1,2]

[1]Institute on Laser and Information Technologies of RAS, Branch of the FSRC "Crystallography and Photonics" RAS 140700 Shatura, Russia
[2]Faculty of Physics and International Laser Center, Lomonosov Moscow State University 119991 Moscow, Russia
[3]Avesta Ltd., 108840 Troitsk, Russia
[4]Budker Institute of Nuclear Physics of the Siberian Branch of RAS 630090 Novosibirsk, Russia
[5]Novosibirsk State University 630090 Novosibirsk, Russia
[*] Corresponding author, soluankp@yandex.ru

Recent advances in sources and detectors development for terahertz (THz) area of electromagnetic spectrum together with variety of potential practical applications (e.g. spectroscopy, imaging, noncontact substance probing, high-speed communications and medicine) leads to the necessity of engineering of compact, cheap and reconfigurable optical elements for THz photonics. For the monochromatic radiation one can use diffractive optics, based on thin films structures. Such elements can be easily reconfigured with the change of optical properties of the film.

One of the promising materials for such device construction is vanadium dioxide (VO_2). Due to the sharp change of conductivity during metal to insulator phase transition, even ultrathin films of this substance can effectively modulate THz radiation. Phase transition can be caused by heating of the sample to temperatures around 68º C, where it becomes conductive. Also, femtosecond pulses of near-infrared radiation can cause phase transition at lower temperatures and sub-picosecond timescales [1].

In our research we have made reconfigurable Fresnel zone plates (FZP) and beamsplitters, based on diffraction gratings, using etched structures in VO_2 films. Films were manufactured using metalorganic chemical vapor deposition (MOCVD) and pulsed laser deposition (PLD) VO_2 growth on wide R-cut sapphire substrates 50 mm or 75 mm in diameter. For the PLD method, metallic vanadium target was illuminated by KrF eximer laser with 15 Hz repetition rate and power density 2.9 J/cm^2. Substrate temperature was kept at 580 C, and oxygen pressure in the chamber was 30 mTorr. After the deposition, samples were annealed at the same conditions for an 1 hour. MOCVD growth was performed in a tubular vertical cold-wall inductively heated reactor by interaction between vanadyl dipivaloylmethanate ($VO(thd)_2$) and water vapors in argon atmosphere at 450˚ C. Device structures were made by standard lithographic processing of wet etching [2]. Substrates with VO_2 films were coated with photo resistive material and exposed by laser beam. Wet etching was performed in 50 vol.% HNO_3. We had achieved etching accuracy better than 10 um.

For the FZP, concentric rings were made. Inner and outer diameters of the rings can be calculated as $r_n = \sqrt{n\lambda F + (0.5\,n\lambda)^2}$, where n is integer, F corresponds to the desired focal length (50 mm and 100 mm) and λ is an QCL wavelength (81 μm for F=3.7 THz). For each structure 7 rings were made, so n_{max}=15. Zone plate example is depicted in Fig. 1. For the beam splitters, diffraction grating was made with the slit width of 80 μm and period of 160 μm.

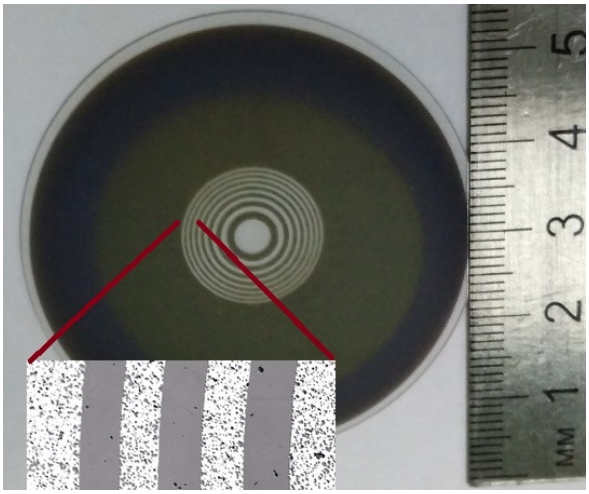

Fig. 1. Zone plate example with F=50 mm at 3.7 THz. Microphotograph for the etching quality is depicted in inset.

We have found PLD films to be 130 nm thick and MOCVD films to be 450 nm thick. DC conductivity changes up to 3.5 orders of magnitude for MOCVD films and 4.5 orders for PLD films during the phase transition. We had measured temperature dependences of THz transmission for several frequencies (0.8 THz TDS, 3.1 and 3.7 THz QCL). These curves have the same form for all measured frequencies, hysteresis width was found to be 4-5 ºC. Transmission contrast, defined as ratio of transmission in isolative state to the transmission in conductive state, decreases with the increase of THz frequency. For 3.1 THz, transmission contrast was up to 85 for MOCVD films and up to 20 for PLD films.

Measurements of the FZP performance were carried out in setup, based on wide beam QCL source. We payed special attention to the spatial structure of initial beam. Device under test was placed in the thermostat. We had measured intensity distributions near focal point of the FZP in both phase states of the film (at 20 and 80 ºC) using 320*240 pixels NEC microbolometer THz camera and Golay cell on 2D-translator. Moreover, numerical simulation within the

frame of the scalar diffraction theory were made. In this calculations, VO_2 structures were considered as semi-transparent screens.

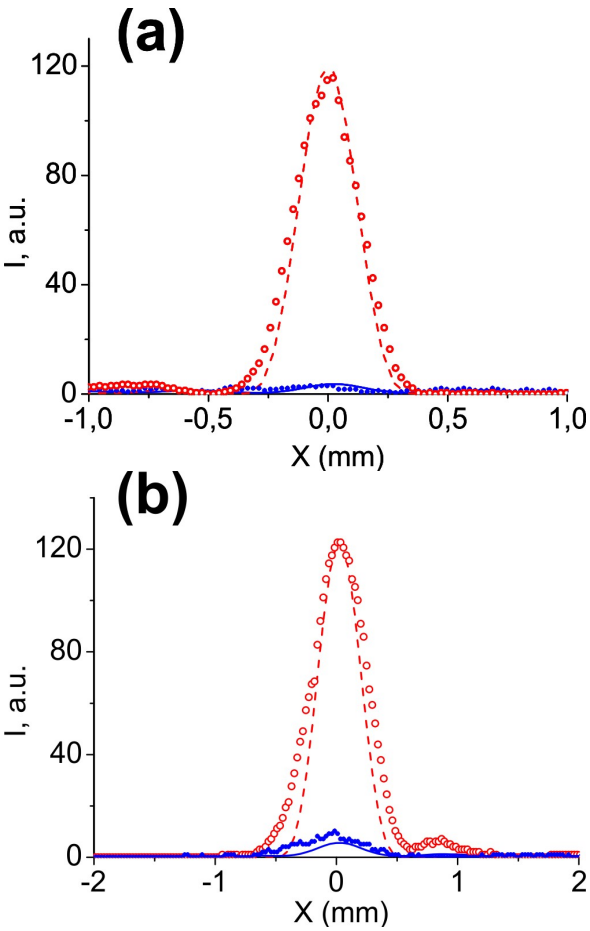

Fig. 2. Intensity distributions in the focal plane for F=50 mm (a) and F=100 mm (b). Filled circles correspond to the low temperature state of the film, open circles – high temperature conductive state. Solid and dashed lines show results for numerical simulations.

We had found measured focal distance of our zone plates equal to the calculated one within 2 mm accuracy of experiment. For the 3.1 THz focal distance had 15% decrease, because FZP were designed for 3.7 THz frequency. Both PLD and MOCVD FZP with the same focal distances showed equal normalized power distributions at the focal plane. Examples of the intensity distribution cross-sections, measured at 3.1 THz for F=50 mm PLD and F=100 mm MOCVD FZPs are presented in Fig. 2. For the PLD FZP we had reached contrast for the peak intensity in two phase states of 38±4, while for MOCVD 16±2. One can see good agreement of the measured and calculated data. Numerical calculations show up to 125-fold increase of peak intensity at focal point comparing to initial beam before FZP. As can be shown from the vector diagram on the complex plane, amplitude of the THz field in the focal point of the ideal FZP would be π times smaller comparing with the ideal refractive lens of the same focal distance and numerical aperture. Our measurements show that power efficiency for FZP is 25±3% of the value for ideal FZP for PLD films and 29±3% for MOCVD films at 3.1 THz. Additional losses are due to the reflection and absorption in 500 μm thick sapphire substrate: it transmits 31±3% of radiation at 3.1 THz and 24±3% at 3.7 THz. Device efficiency can be improved with the use of antireflective coating [3] and thinner substrates.

To test beamsplitters, we had measured angular distribution of the THz intensity after passing through diffraction grid. We had observed symmetrical picture with 0-th and 1-st order diffraction maxima. Intensity contrast in 1-st order maximum between two phase states was as high as 68. In the conductive state of the film, intensity in each 1-st order maximum was 16% of intensity in zero order maximum. Simple theory shows that varying grating geometry one can achieve splitting ratio up to 1:1:1.

To test the possibility of optical modulation of our devices we had illuminated our films with high-power femtosecond and CW radiation at 800 nm wavelength. We had found breakdown threshold at 10 mJ/cm^2 for 120-fs pulses. Maximum photoinduced absorption was measured to be 0.6 of the transmitted radiation with characteristic timescales around 1 ps.

In conclusion, we have proposed and examined reconfigurable THz elements for QCL radiation such as beam splitters and FZPs, based on VO_2 films with various properties. For FZP, we had achieved modulation of intensity in the focal point up to 38 times with power efficiency up to 29% of the value for ideal amplitude zone plate. We had investigated the possibility of optical modulation for such elements and influence of VO_2 film properties on device performance.

We appreciate teams from Kurchatov institute (M. L. Zanaveskin, I. A. Chernykh, I. V. Kulikov) and from MSU, Faculty of Chemistry (A. R. Kaul, A. M. Makarevich, D. I. Sharovarov) for VO_2 film growth using PLD and MOCVD techniques respectively. Work was supported by the Russian Foundation for Basic Research under project no. 16-29-11800 ofi-m and 15-33-70026 mol-a-mos.

References

1. Cocker, T. L., Titova, L. V., Fourmaux, S., Holloway, G., Bandulet, H. C., Brassard, D., ... & Hegmann, F. A. Phase diagram of the ultrafast photoinduced insulator-metal transition in vanadium dioxide // Physical Review B 2012, V. 85 No. 15, P. 155120.

2. Jostmeier, T., Zimmer, J., Karl, H., Krenner, H. J., Betz, M. Optically imprinted reconfigurable photonic elements in a VO2 nanocomposite // Appl. Phys. Lett. 2014, V. 105 No. 7, P. 071107.

3. Agafonov, A. N., Volodkin, B. O., Kaveev, A. K., Knyazev, B. A., Kropotov, G. I., Pavel'ev, V. S., ... & Choporova, Y. Y. Silicon diffractive optical elements for high-power monochromatic terahertz radiation// Optoelectronics, Instrumentation and Data Processing 2013, V. 49 No. 2, P. 189-195.

Quantum-cascade lasers of mid-IR spectral range: epitaxy, diagnostics and device characteristics

A. V. Babichev[1], A. G. Gladyshev[2], E. S. Kolodeznyi[1], A. S. Kurochkin[1], G. S. Sokolovskii[3], V. E. Bougrov[1], L. Ya. Karachinsky[1,2,3], I. I. Novikov[1,2,3], V. V. Dudelev[3], V. N. Nevedomsky[3], S. O. Slipchenko[3], A. V. Lutetskiy[3], A. N. Sofronov[4], D.A. Firsov[4], L.E. Vorobjev[4], N. A. Pikhtin[3], A. Bousseksou[5], A. Yu. Egorov[1]

[1]ITMO University, St. Petersburg, Russia, a.babichev@corp.ifmo.ru
[2]Connector Optics LLC, St. Petersburg, Russia
[3]Ioffe Institute, St. Petersburg, Russia
[4]Peter the Great St. Petersburg Polytechnic University, St. Petersburg, Russia
[5]Center of Nanoscience and Nanotechnology (C2N), Universit´e, Paris Sud and Paris-Saclay, Orsay cedex, France

Since the first practical realization of quantum-cascade lasers (QCL) the considerable progress has been achieved in the theory, epitaxy, and laser formation. Growth of QCL lasers by metal-organic chemical vapour deposition instead of molecular beam epitaxy (MBE) has been demonstrated [1,2]. The using of MBE increases the efficiency of QCL mainly due to the possibility to grow high quality identical multiperiod superlattices. Smooth control of epitaxial growth rate during the growth of QCL heterostructures [3,4] and/or using of cell with increased stability of the fluxes of elements of Group III [5,6] allow increasing the identity of QCL cascades. In this paper we report on epitaxy, diagnostics and device characteristics of QCL heterostructures grown using the industrial MBE system Riber 49 utilizing the ABI 1000 cells with a cylindrical crucible.

The first design (type 1) with the active region based on bound-to-continuum design [7,8] was suggested for lasing at ~ 6 μm. Before forming the stages of the laser on an InP substrate, an 100 nm $In_{0.53}Ga_{0.47}As$ buffer layer doped by silicon (Si) and lattice matched to InP was grown. The heterostructure contains 60 stages formed by the strain-compensated $In_{0.44}Al_{0.56}As/In_{0.60}Ga_{0.40}As$ heteropair that provided the necessary elastic balance in the QCL stages and a band offset ΔE_c of more than 630 meV at the heterointerface. The $In_{0.52}Al_{0.48}As$ top cladding layer and $In_{0.53}Ga_{0.47}As$ contact layer doped by Si have thickness of 1500 and 50 nm, respectively.

The active region design with the escape of charge carriers due to two-phonon resonance was used for 8 μm spectral range QCL heterostructure and consisted of 50 stages based on the $In_{0.53}Ga_{0.47}As/Al_{0.48}In_{0.52}As$ heteropair lattice matched to InP substrate. It was developed three waveguide types in 8 μm spectral range QCL heterostructures. First of them (type 2A) consisted of bottom cladding based on InP (2 μm thick) and $In_{0.53}Ga_{0.47}As$ (0.5 μm thick) layers, which were grown on a substrate in succession, the active region including 50 stages and $In_{0.53}Ga_{0.47}As$ layers of top cladding with 1×10^{17} cm^{-3} and 1×10^{19} cm^{-3} doping levels and with thickness of 0.1 μm and 0.02 μm, respectively [9,10]. Second of them (type 2B) was based on the bottom $In_{0.53}Ga_{0.47}As$ waveguide layer (0.5 μm thick), active region layers, top cladding layers based on InP (0.75 μm thick), waveguide based $In_{0.53}Ga_{0.47}As$ and contact $In_{0.53}Ga_{0.47}As$ layers with 1×10^{17} cm^{-3} and 1×10^{19} cm^{-3} doping level with thicknesses of 0.1 μm and 0.02 μm, respectively. Third of them (type 2C) consisted of bottom $In_{0.53}Ga_{0.47}As$ waveguide layer (0.5 μm thick), active region layers, top cladding layers based on InP (3.9 μm thick) and waveguide based on $In_{0.53}Ga_{0.47}As$ and contact $In_{0.53}Ga_{0.47}As$ layers with 1×10^{17} cm^{-3} and 1×10^{19} cm^{-3} doping level with thicknesses of 0.1 μm and 0.02 μm, respectively.

The three-phonon resonance design [5] was used for 9 μm spectral range QCL heterostructure (type 3) and consisted of 40 periods based on $In_{0.53}Ga_{0.47}As$ quantum wells with $Al_{0.48}In_{0.52}As$ barrier layers. Heterostructure consisted of $In_{0.53}Ga_{0.47}As$: Si (with 1×10^{18} cm^{-3} doping level) current spreading layer with a thickness of 50 nm, bottom cladding $In_{0.53}Ga_{0.47}As$: Si layer with 5×10^{16} cm^{-3} doping level and 4 μm thick active region layers, top cladding layers (4 μm thick) based on step-doped $Al_{0.48}In_{0.52}As$:Si ($1 \times 10^{17}/1 \times 10^{18}$ cm^{-3}) and 0.2 μm thick contact layer of $In_{0.53}Ga_{0.47}As$: Si (5×10^{18} cm^{-3}).

The heterostructure of the dual-frequency QCL (type 4) consisted of $In_{0.53}Ga_{0.47}As$: Si (with 1×10^{18} cm^{-3} doping level) current spreading layer with a thickness of 50 nm, bottom cladding $In_{0.53}Ga_{0.47}As$: Si layer with 5×10^{16} cm^{-3} doping level (2.1 μm thick), sequence of 15 stages of type 2 active region, sequence of 36 stages of type 3 active region, sequence of 15 stages of type 2 active region, top cladding layers based on $In_{0.53}Ga_{0.47}As$ (1.95 μm thick) and $In_{0.52}Al_{0.48}As$ (2 μm thick) and 0.02 μm thick contact layer of $In_{0.53}Ga_{0.47}As$: Si with 1×10^{19} cm^{-3} doping level.

X-ray diffraction measurements showed narrow satellite peaks, which indicate high structural perfection of the multi-stage QCL heterostructures. The spectra of X-ray diffraction were measured with high resolution in the vicinity of the InP symmetrical (004) reflection using a PANanalytical X'PertPro diffractometer with parallel geometry of the X-ray radiation beam. Additional analysis of high-resolution transmission electron microscopy (TEM) proved the absent of extended defects and that all layers have planar heteroboundaries. The TEM studies were conducted at a JEM2100F transmission electron microscope with an accelerating voltage of 200 keV.

The heterostructures of QCL were processed in four-cleaved and ridge geometries and mounted on

copper heatsink using the indium solder to study the spontaneous and stimulated emission.

The QCL of type 1 based on strained heteropair $In_{0.44}Al_{0.56}As/In_{0.60}Ga_{0.40}As$ with $Al_{0.48}In_{0.52}As$ top cladding has shown the room-temperature lasing at threshold current density of 4.8 kA/cm^2 with the peak emission wavelength about 5.8 μm [3]. The estimated output optical power from one facet was about 150 mW in pulse mode.

The QCL of type 2A (waveguide with air cladding) demonstrated the lasing at room temperature with the threshold current density about 5.1 kA/cm^2 [9]. The lasing spectra demonstrate maximum close to 8 μm. The same QCL with full top metallization demonstrate the lasing up to 250 K with the threshold current density about 5 kA/cm^2 [11].

The QCL of type 2B (waveguide with thin top cladding) demonstrated the lasing at room temperature and the threshold current density about 5.6 kA/cm^2. The lasing wavelength was close to 7.8 μm. The estimated output peak optical power measured at 300 K was about 100 mW.

The QCL of type 2C (waveguide with thick top cladding) demonstrated the lasing at room temperature with wavelength 8.0 μm and the threshold current density about 4.9 kA/cm^2. The estimated output peak optical power measured at 300 K was about 200 mW.

For type 3 QCL the lasing up to 140 K was demonstrated. Threshold current density determined at 87 K was about 3 kA/cm^2. The estimated output optical power is about 20-35 mW, measured from one facet in pulse mode [5].

The heterostructure of dual-frequency QCL based on type 3 design was created and its structural and optical quality was studied. The design of waveguide with uniform pumping of both active regions [12] was implemented in this heterostructure. The realization of waveguide based on 2 active region one emitting at 7.6 μm wavelength and separated by other active region emitting at wavelengths of 9.6 μm allows to reach the lasing close to 7.6 μm and well pronounce of spontaneous emission near 9.6 μm.

To summarize, we presented the results of the study of QCL with different active region inside 5-10 μm spectral range. Room temperature lasing with output optical power about a few hundreds of milliwatt was demonstrated. The further optimization should be related with usage of thick InP top cladding and decreasing of injector doping level aimed to reach low threshold current density that is necessary for the high-power continuous-wave lasing.

This was supported by the Ministry of Education and Science of the Russian Federation within the Federal target program “Research and Development in Priority Areas of the Science and Technology Complex of Russia for 2014–2020”, code no. 2016-14-579-0009, unique identifier RFMEFI57816X0204.

References

1. *Wang, C. A., Schwarz, B., Siriani, D. F., Missaggia, L. J., Connors, M. K., Mansuripur, T. S., Calawa, D. R., McNulty, D., Nickerson, M., Donnelly, J. P., Creedon, K.* MOVPE growth of LWIR AlInAs/GaInAs/InP quantum cascade lasers: Impact of growth and material quality on laser performance // IEEE J. Sel. Top. Quantum Electron. 2017. V. 23, No. 6. P. 1-13.

2. *Zasavitskii, I. I., Kovbasa, N. Y., Raspopov, N. A., Lobintsov, A. V., Kurnyavko, Y. V., Gorlachuk, P. V., Krysa A.B., Revin, D. G.* // A GaInAs/AlInAs quantum cascade laser with an emission wavelength of 5.6 μm // Quantum Electron. 2018. V. 48, No. 5. P. 472–475.

3. *Babichev, A. V., Bousseksou, A., Pikhtin, N. A., Tarasov, I. S., Nikitina, E. V., Sofronov, A. N., Firsov D. A., Vorobjev L. E., Novikov I. I., Karachinsky L. Y., Egorov, A. Y.* Room-temperature operation of quantum cascade lasers at a wavelength of 5.8 μm // Semiconductors 2016. V. 50, No. 10. P. 1299–1303.

4. *Mamutin, V. V., Vasilyev, A. P., Lyutetskiy, A. V., Ilyinskaya, N. D., Zadiranov, Y. M., Sofronov, A. N., Firsov, D. A., Vorobjev, L. E., Maleev, N. A., Ustinov, V. M.* On the Fabrication and Study of Lattice-Matched Heterostructures for Quantum Cascade Lasers // Semiconductors 2018. V. 52, No. 7. P. 950–953.

5. *Babichev, A. V., Gusev, G. A., Sofronov, A. N., Firsov, D. A., Vorobjev, L. E., Usikova, A. A., Zadiranov, Yu. M., Il'inskaya, N. D., Nevedomsky, V. N., Dudelev, V. V., Sokolovskii, G. S., Gladyshev, A. G., Karachinsky, L. Ya., Novikov, I. I., Egorov A. Yu.* Lasing of quantum-cascade laser at 9.6 μm wavelength // Tech. Phys. 2018. V. 88, No. 10, in press.

6. *Babichev, A. V., Gladyshev, A. G., Filimonov, A. V., Nevedomskii, V. N., Kurochkin, A. S., Kolodeznyi, E. S., Sokolovskii, G. S., Bugrov, V. E., Karachinsky, L. Ya., Novikov, I. I., Bousseksou, A., Egorov, A. Yu.* Heterostructures for quantum-cascade lasers of the wavelength range of 7–8 μm // Tech. Phys. Lett. 2017. V. 43, No. 7. P. 666–669.

7. *Faist, J., Beck, M., Aellen, T., Gini, E.* Quantum-cascade lasers based on a bound-to-continuum transition // Appl. Phys. Lett. 2001. V. 78, No. 2. P. 147–149.

8. *Egorov, A. Y., Babichev, A. V., Karachinsky, L. Y., Novikov, I. I., Nikitina, E. V., Tchernycheva, M., Tchernycheva, M., Sofronov, A. N., Firsov, D. A., Vorobjev, L. E., Pikhtin, N. A., Tarasov, I. S.* Lasing of multiperiod quantum-cascade lasers in the spectral range of (5.6–5.8)-μm under current pumping // Semiconductors 2015. V. 49, No. 11. P. 1527–1530.

9. *Babichev, A. V., Gladyshev, A. G., Kurochkin, A. S., Kolodeznyi, E. S., Sokolovskii, G. S., Bougrov, V. E., Karachinsky L. Ya., Novikov I. I., Bousseksou A., Egorov, A. Y.* Room Temperature Lasing of Multi-Stage Quantum-Cascade Lasers at 8 μm Wavelength // Semiconductors 2018. V. 52, No. 8. P. 1082–1085.

10. *Babichev, A. V., Gladyshev, A. G., Filimonov, A. V., Nevedomskii, V. N., Kurochkin, A. S., Kolodeznyi, E. S., Sokolovskii, G. S., Bugrov, V. E., Karachinsky, L. Ya., Novikov, I. I., Bousseksou, A., Egorov, A. Y. Heterostructures for quantum-cascade lasers of the wavelength range of 7–8 μm* // Tech. Phys. Lett. 2017. V. 43, No. 7. P. 666–669.

11. *Kurochkin, A. S., Babichev, A. V., Denisov, D. V., Karachinsky, L. Y., Novikov, I. I., Sofronov, A. N., Firsov, D. A., Vorobjev, L. E., Bousseksou, A., Egorov, A. Yu.* Quantum-cascade lasers in the 7-8 μm spectral range with full top metallization // J. Phys.: Conf. Ser. 2018. V. 993, No. 1. P. 012031.

12. *Babichev, A. V., Kurochkin, A. S., Kolodeznyi, E. C., Filimonov, A. V., Usikova, A. A., Nevedomsky, V. N., Gladyshev, A. G., Karachinsky, L. Ya., Novikov, I. I., Egorov, A. Yu.* Heterostructures of Single-Wavelength and Dual-Wavelength Quantum-Cascade Lasers // Semiconductors. 2018. V. 52, No. 6. P. 745–749.

Terahertz quantum cascade lasers with silver- and gold-based waveguides

R. A. Khabibullin[1], N. V. Shchavruk[1], D.S. Ponomarev[1], D.V. Ushakov[2], A.A. Afonenko[2], O.Yu. Volkov[3], V.V. Pavlovskiy[3], A.A. Dubinov[4]

[1]V.G. Mokerov Institute of Ultra High Frequency Semiconductor Electronics of RAS, Moscow, Russia, khabibullin@isvch.ru
[2]Belarusian State University, Minsk, Belarus
[3]Institute of radio-engineering and electronics of RAS, Moscow, Russia
[4]Institute for Physics of Microstructures RAS, Nizhny Novgorod, Russia

For the practical use of THz quantum cascade lasers (QCLs) in a large field of applications, including real-time THz imaging and THz spectroscopy, it is necessary to develop low loss waveguides [1].The most efficient in the THz region of the spectrum is a double metal waveguide (DMW) design in which the active region is placed between two metal layers. The mode confinement factor in such waveguides is $\Gamma \sim 1$, which is much higher than in plasmon waveguides ($\Gamma \sim 0.3$), which effectively work for mid-infrared QCLs. However, QCLs with DMW are complex in fabrication [2] and require preliminary theoretical and experimental studies of the behavior of the dielectric constant and the loss coefficient of both metals and semiconductors in the THz spectral region.

For the development of more efficient laser schemes for THz QCLs, as well as a low loss waveguide design, the information is needed on the loss in THz QCLs over a wide range of temperatures and frequencies. It is shown that the loss in THz QCLs plays an important role in the internal tuning of the radiation frequency [3]. In this work, we propose to use a double metal waveguide based on silver (Ag), for reducing the losses of the waveguide. In comparison with Au, Ag has a higher electrical and thermal conductivities, which should lead to low losses in the Ag-based waveguide. For this purpose, we investigate the spectra of mode losses in THz QCL with DMW based on Au and Ag.

Metal film of Ti/Au (30/1000 nm) and Ti/Ag (30/1000 nm) are deposited on SI-GaAs, and their resistivities are measured using Van der Pauw method in the temperature range from 4.2 to 300 K. The dielectric constants and loss coefficients (α_{met}) are calculated on the basis of measurements of the resistivity of metals using the Drude model. As shown in Fig. 1, the loss coefficient on the Au- and Ag-based DMW increases with increasing frequency and temperature. Using Ag for DMW allows to reduce α_{met} by more than 2 cm^{-1} comparing with DMW based on Au.

Calculations of the coefficient of total losses, including losses on the DMW, resonator mirrors, optical phonons and free charge carriers, are performed for a 10-μm waveguide. It is demonstrated that, taking into account the absorption of THz radiation by free carriers and optical phonons (see the inset of Fig. 2), the spectrum of total mode losses has a wide minimum in the region of 3-6 THz, which shifts to the high-frequency region of the spectrum with increasing temperature (see Fig. 2). The minimum losses in an Au-based waveguide with an increase of temperature from 100 to 300 K increase from 8 to 27 cm^{-1}. The use of Ag-based DMW allows to reduce losses by 2–4 cm^{-1} in comparison with Au-based DMW.

We have designed the active region of the THz QCL based on three tunnel-coupled quantum wells $GaAs/Al_{0.15}Ga_{0.85}As$ with a resonance-phonon depopulation scheme [4]. Numerical calculations of energy levels, matrix elements of dipole transitions, the degree of subbands populations and gain spectra are carried out depending on the applied electric field and temperature. It is shown that the maximum gain is realized under phonon resonance conditions at a frequency of 3.37 THz at an electric field strength of F = 12.3 kV/cm [5].

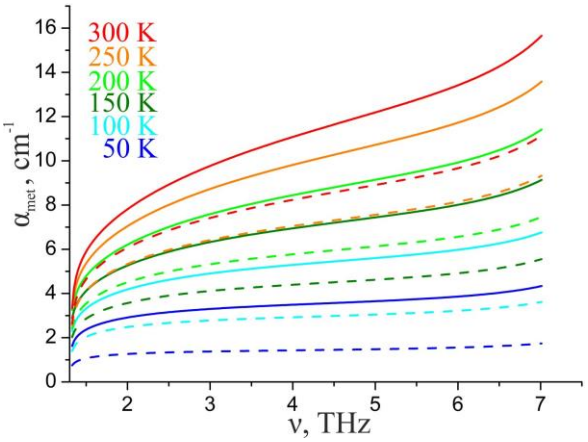

Fig. 1. The spectra of the loss coefficient on the Au-based DMW (solid lines) and Ag-based DMW (dashed lines) at temperatures from 50 to 300 K.

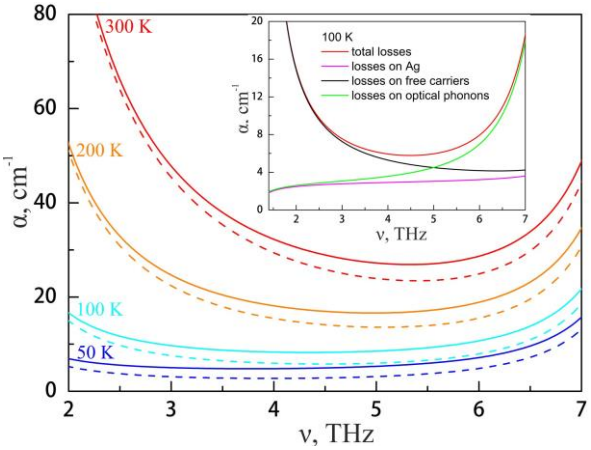

Fig. 2. Total losses of THz QCL with DMW based on Au and Ag for different temperatures. The inset shows the components for the total loss coefficient for THz QCL based on Ag DMW at 100 K.

Based on the proposed design, the laser heterostructures are grown by molecular beam epitaxy with 10 μm active region thickness [6]. We fabricate ridge structures with Au-based DMW [7]. The device is die bonded to a copper submount with wire bonding to ridge structures. Measurements are made with an abutted to laser facet sapphire hyperhemispherical lens.

The lasing threshold of the fabricated THz QCL is achieved at a current of 0.85–0.86 A for 20 K. The influence of temperature on the threshold current and output power of the fabricated THz QCL emitting near ~ 3.3 THz with a maximum operating temperature of T_{max} ~ 84 K is investigated. By fitting the dependence of threshold current J_{th} on temperature to the empirical expression $J_{th} \sim \exp(T/T_0)$, we obtain the characteristic temperature T_0 = 20 K for fabricated THz QCL. It is seen that with an increase in temperature from 40 to 58 K, an insignificant decrease in the THz QCL radiation power by ~ 35%, which allows the pumping of nitrogen vapors to be used to cool the laser. The characteristic energy of E_a = 23 meV, which is necessary for the temperature activation of LO phonon emission in the case of electron recombination from the upper laser level to the lower one, is determined from the Arrhenius temperature dependence of the output power.

In measured at 58 K spectrums, there are three equidistant spectral lines corresponding to the longitudinal Fabry-Perot modes with $\Delta f = c/2nL$ = 40 GHz for L=1 mm. The mode content varies with the bias current. There are three radiation modes (3.24, 3.28, 3.32 THz) at a pumping current of 0.940 A. Generation at 3.32 THz ceases when the current increases to 1.005 A, and only two high-frequency modes remain at 1.058 A. The maximum amplitude of the total radiation power is 28 μW in the 3.25–3.32 THz range at a temperature of 42 K [8].

We investigate the post-growth processing for THz QCL with Ag-based DMW. This processing includes the Ag–Ag thermocompression bonding of QCL heterostructures with a doped n+-GaAs substrate, mechanical lapping and selective wet etching of the substrate, and dry etching of QCL ridge structures through a Ti/Ag/Au metallization mask 100 μm wide. Reactive-ion-etching recipe with an inductively coupled plasma source in a BCl_3/Ar gas mixture is selected to obtain vertical walls of the QCL ridge structure with minimum Ti/Ag/Au mask sputtering (Fig. 6).

Conclusion

The coefficient of total losses of THz QCL with DMW based on Au and Ag have been analyzed. We have designed and fabricated THz QCLs with Au-DMW based on $GaAs/Al_{0.15}Ga_{0.85}As$ three-quantum well active module with resonant-phonon depopulation scheme. We investigate the dependence of threshold current and lasing output power on temperature. The dependence of the radiation spectrum on the amplitude of the excitation current pulse was investigated. The postgrowth processing for THz QCL with Ag-based DMW are studied.

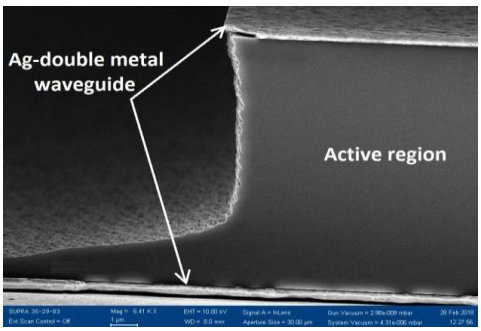

Fig. 3. SEM image of THz QCL with Ag-Ag double metal waveguide.

Acknowledgements

This work was supported by the Russian Science Foundation (Project #18-19-00493).

References

1. *Han, Y. J., Li, L.H., Zhu, J., Valavanis, A., Freeman, J.R., Chen, L., Rosamond, M., Dean, P., Davies, A.G., Linfield, E.H.* Silver-based surface plasmon waveguide for terahertz quantum cascade lasers // Opt. Express. 2018. V. 26, No.4. P. 3814-3827.

2. *Khabibullin, R. A., Shchavruk, N. V., Pavlov, A. Y., Ponomarev, D. S., Tomosh, K. N., R. R. Galiev, Maltsev, P. P., Zhukov, A. E., Cirlin, G. E., Zubov, F. I., Alferov, Z. I.* Fabrication of a terahertz quantum-cascade laser with a double metal waveguide based on multilayer GaAs/AlGaAs heterostructures // Semiconductors. 2016. V. 50, No. 10. P. 1377–1382.

3. *Schrottke, L., Lu, X., Roben, B., Biermann, K., Wienold, M., Richter, H., Hubers, H.W., Grahn. H.T.* Intrinsic frequency tuning of terahertz quantum-cascade lasers // J. Appl. Phys. 2018. V. 123, No. 21. P. 213102.

4. *Khabibullin, R. A., Shchavruk, N. V., Ponomarev, D. S., Ushakov, D. V., Afonenko, A. A., Vasil'evskii, I. S., Zaycev, A. A., Danilov, A. I., Volkov, O. Yu., Pavlovskiy, V. V., Maremyanin, K. V., Gavrilenko, V. I.* Temperature dependences of the threshold current and output power of a quantum-cascade laser emitting at 3.3 THz // Semiconductors. 2018. V. 52, No. 11. P. 1381–1386.

5. *Khabibullin, R. A., Shchavruk, N. V., Klochkov, A. N., Glinskiy, I. A., Zenchenko, N. V., Ponomarev, D. S., Maltsev, P. P., Zaycev, A. A., Zubov, F. I., Zhukov, A. E., Cirlin, G. E., Alferov, Zh. I.* Energy spectrum and thermal properties of a terahertz quantum-cascade laser based on the resonant-phonon depopulation scheme // Semiconductors. 2017. V. 51, No. 4. P. 514–519.

6. *Reznik, R. R., Kryzhanovskaya, N. V., Zubov, F. I., Zhukov, A. E., Khabibullin, R. A., Morozov, S. V., Cirlin G. E.* MBE growth, structural and optical properties of multilayer heterostructures for quantum-cascade laser // Journal of Physics: Conf. Series. 2017, V. 917. P. 052012

7. *Ikonnikov, A. V., Marem'yanin, K. V., Morozov, S. V., Gavrilenko, V. I., Pavlov, A. Yu., Shchavruk, N. V., Khabibullin, R. A., Reznik, R. R., Cirlin, G. E., Zubov, F. I., Zhukov, A. E., Alferov, Zh. I.* Terahertz radiation generation in multilayer quantum-cascade heterostructures // Technical Physics Letters. 2017, V. 43, No. 4. P. 358-361.

8. *Volkov, O. Yu., Dyuzhikov, I. N., Logunov, M. V., Nikitov, S. A., Pavlovskii, V. V., Shchavruk, N. V., Pavlov, A. Yu., Khabibullin, R. A.* Analysis of terahertz radiation spectra in multilayer GaAs/AlGaAs heterostructures // Journal of Communications Technology and Electronics. 2018. Vol. 63, No. 9. P. 1042–1046.

Overview of Techniques for THz QCL phase-locking

A. Khudchenko[1,2], D.G.Pavelev[3], V.L Vaks[4], A.M. Baryshev[1,5]

[1]Kapteyn Astronomical Institute/NOVA, University of Groningen, Groningen, Netherlands, a.khudchenko@sron.nl
[2]Kotel'nikov Institute of Radio Engineering and Electronics RAS, Moscow, Russia
[3]Lobachevsky State University, Nizhny Novgorod, Russia
[4]Institute for Physics of Microstructures RAS, Nizhny Novgorod, Russia
[5]Astro Space Center, Lebedev Physical Institute of Russian Academy of Science, Moscow, Russia

Since the first demonstration of a THz Quantum Cascade Laser (QCL) in 2002 [1] it was rapidly improved towards practical applications, for example THz imaging [2] and molecular spectroscopy [3] with high resolution.

At the moment, QCL is one of the most attractive continuous wave (CW) sources in the frequency range of 3-6 THz for heterodyne spectroscopy. In the terahertz astronomy QCLs are used as LO sources in heterodyne receivers for projects SOFIA [4] and GUSTO [5] and are considered for space observatories such as Millimetron [6], LOCUS [7] and OST [8]. Frequency stability of LO is absolutely crucial for a heterodyne instrument because it influences the quality of scientific data delivered by the receiver. The most reliable option to stabilize the LO frequency is phase-locking. Phase-locking of a THz QCL has been demonstrated by various groups using various methods. Here we make an overview of these techniques.

The first frequency stabilization was demonstrated by Betz *et al.* in 2005 [9] by frequency-locking (and partial phase-locking) of 3 THz 1 mW QCL to a far-infrared (FIR) gas laser using GaAs Schottky mixer. A while later, in 2006 Baryshev *et al.* [10] showed phase-locking of two-mode QCL, using an inter-mode beat signal generated on hot-electron bolometer mixer (HEB). Both these experiments were important demonstration of QCL stabilization, though they were difficulties for practical applications.

Afterwards, in 2009 Rabanus *et al.* [11] and Khosropanach *et al.* [12] showed independently stable phase-locking for single-tone QCL, in [11] it was used 1.5 THz 0.3 mW laser and in [12] – 2.7 THz 0.38mW one. The key moment is that both groups used HEB mixer to generate the beat signal for phase locking loop (PLL) system. The reference RF signal in [11] was generated by a high power multiplying chain able to pump an HEB mixer, while in [12] was used a frequency comb generated by superlattice diode mixer [13] pumped by 182 GHz microwave source. A little later, in 2010 Consolino *et al.* [14] realized similar approach for phase-locking of 2.5 THz 1 mW QCL, using HEB mixer, though the reference RF reference was a COMB signal generated by the Cherenkov effect in a lithium niobate waveguide effected by Ti:sapphire femtosecond laser. These three phase-locking approaches [11][12][14] can be combined in one group show schematically on fig.1, utilizing HEB mixer, which is known to be the most sensitive mixer from 1.5 to 6 THz. Nether the less, presence of HEB an in the locking scheme means arranging a separate 4K cryostat. It is not an issue for lab experiments, but it makes serious complications for on-bard application of a locking system.

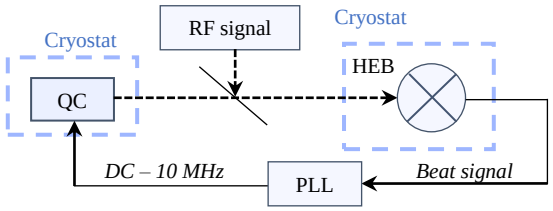

Fig. 1. Simplified block-diagram of QCL phase-locking described in papers [11], [12] and [14]. In all the cases the HEB mixer is used to provide a beat signal between the QLC and a reference signal. The RF signals in all the approaches are generated in different way.

In 2010 Barbiere *et al.* [15] demonstrated another approach of QCL phase-locking. In this experiment, a mode-locked femtosecond laser and a QCL radiation (2.7 THz, power of 25 mW) were applied to electro-optic detection system. This photo-mixing system generated a mixing product between a QCL frequency and the n_{th} harmonic of repetition rate of femtosecond laser of 90 MHz. The photocurrent beat signal frequency was 30 MHz. The electro-optic detection system is based on ZnTe crystal modulating amplitude of femtosecond pulses with the QCL frequency and on high speed (bandwidth of 300 MHz) silicon photodiodes. Similar technique was used a year later in 2011 by Ravaro *et al.* [16] to phase-lock 10mW QCL radiating at 2.5 THz (see fig. 2).

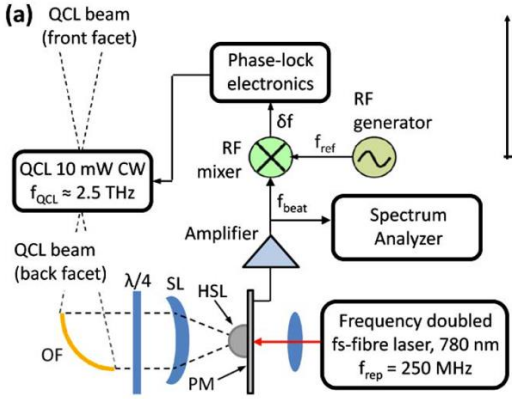

Fig. 2. Block-diagram of QCL phase-locking taken form [16]. THz field from the QCL is mixed with the photocarrier THz comb induced in the PM by the fs pulse train generated in fiber laser with repetition rate of 250 MHz.

The main new element relative to [15] is a GaAs photomixer. A big advantage of scheme in [15] and [16] is that only a room-temperature-operated elements are used. A fiber laser technology and the semiconductor

photomixer are much more light and compact than superconducting bolometer mixers.

Another way of QCL phase-locking has been described in 2013 by Hayton *et al.* [17]. The authors phase locked a 3.4 THz 1 mW distributed feedback (DFB) laser to the 18th harmonic of a 190.7 GHz reference source using a room temperature GaAs/AlAs superlattice diode. Next year Khudchenko *et al.* [18] employed the same technique for 4.7 THz 0.25 mW QCL. The key element of this scheme (see fig. 3) is the harmonic mixer receiving QCL signal and mixing it with n_{th} harmonic of a reference microwave signal of about 10 mW power at frequency around 200 GHz. The product is used by PLL system to control phase and frequency of QCL. All the elements of the locking loop are working at room temperature. A very similar approach, but using Schottky harmonic mixer instead of super-lattice one, was been published in 2015 by Danylov *et al.* [19] and Bulcha *et al.* [20]. In [20] it was phase locked a 2.5 THz laser, and in [19] – 2.3 THz and 2.9 THz lasers of power correspondingly. All the experiments in [17], [18], [19] and [20] can be reflected by very simple scheme shown in fig. 3.

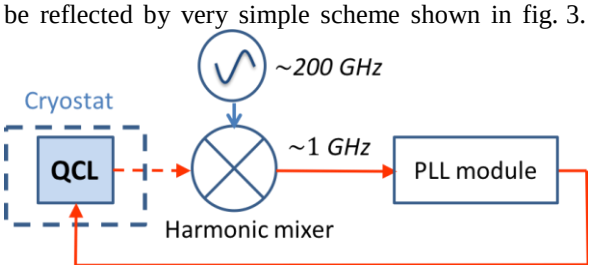

Fig. 3. Simplified block-diagram of QCL phase-locking shown in [17], [18], [19] and [20].

The latest conceptually unique method of QCL phase locking was presented in 2017 by Freeman *et al.* [21]. The 2 THz 1.7 mW QCL was locked not by an active feed-back system but by injection locking method. Employing infrared frequency combs and InGaAs photomixers a reference signal of 100 nW was generated at frequency very close to the QCL frequency. This signal was injected into the QCL and synchronized its radiation.

To summarize, the most promising are four techniques: [15]/[16]; [17]/[18] ; [19]/[20] and [21].

However, only in [18] it was shown phase locking at 4.7 THz, all the other QCLs are below 3 THz. Though, one of the most interesting applications for QCL is a role of LO in on-board heterodyne receiver at 4.7 THz to observe atomic oxygen line [4-8].

References

[1] *R. Köhler, A. Tredicucci, et. al. //* Terahertz semiconductor heterostructure laser // Nature 417, 156–159, 2002.

[2] *A. W. M. Lee, Q. Qin, et al.* // "Real-time terahertz imaging over a standoff distance (>25 meters) // Appl. Phys. Lett. ,89, 141125, 2006.

[3] *H.-W. Hübers, S. G. Pavlov, et. al.* // High-resolution gas phase spectroscopy with a distributed feedback terahertz quantum cascade laser // Appl. Phys. Lett. 89, 061115 2006.

[4] *H. Richter, M. Weinold, et al //* 4.7-THz Local Oscillator for the GREAT Heterodyne Spectrometer on SOFIA // IEEE Trans. on TST 5, 539-535, 2015.

[5] *https://www.sron.nl/missions-astrophysics/gusto*

[6] *http://millimetron.ru/index.php/en/*

[7] *http://www.locussatellite.com/*

[8] *J. Fortney et al. https://arxiv.org/abs/1803.07730*

[9] *A. L. Betz, R.T. Boreiko, et al.* // Frequency and phase-lock control of a 3 THz quantum cascade laser // Opt. Lett. 30, 1837-1839, 2005

[10] *A. Baryshev, J. N. Hovenier, A. J. L. Adam, I. Kaalynas, J. R. Gao, T. O. Klaassen, B. S. Williams, S. Kumar, Q. Hu, and J. L. Reno* // Phase locking and spectral linewidth of a two-mode terahertz quantum cascade laser // Appl. Phys. Lett. 89, 031115 , 2006.

[11] *D. Rabanus, U. U. Graf, M. Philipp, O. Ricken, J. Stutzki, B. Vowinkel, M. C. Wiedner, C. Walther, M. Fischer, and J. Faist* // Phase locking of a 1.5 Terahertz quantum cascade laser and use as a local oscillator in a heterodyne HEB receiver // Opt. Express 17, 1159-1168, 2009.

[12] *P. Khosropanah, A. Baryshev, W. Zhang, W. Jellema, J. N. Hovenier, J. R. Gao, T. M. Klapwijk, D. G. Paveliev, B. S. Williams, S. Kumar, Q. Hu, J. L. Reno, B. Klein, and J. L. Hesler* // Phase locking of a 2.7 THz quantum cascade laser to a microwave reference // Opt. Lett. 34, 2958–2960 , 2009.

[13] *D. G. Paveliev, Yu. I. Koschurinov, V. M. Ustinov, A. E. Zhukov, F. Lewen, C. Endres, A. M. Baryshev, P. Khosropanah, W. Zhang, K. F. Renk, B. I. Stahl, A. Semenov, and H.-W. Huebers* // conf. proc., ISSTT, 319, 2008.

[14] *L. Consolino, A. Taschin, P. Bartolini, S. Bartalini, P. Cancio, A. Tredicucci, H. E. Beere, D. A. Ritchie, R. Torre, M. S. Vitiello, and P. De Natale* // Phase-locking to a free-space terahertz comb for metrological-grade terahertz lasers // Nat. Commun. 3, 1040.

[15] *S. Barbieri, P. Gellie, G. Santarelli, L. Ding, W. Maineult, C. Sirtori, R. Colombelli, H. Beere, and D. Ritchie //* Phase-locking of a 2.7, THz quantum cascade laser to a mode-locked erbium-doped fibre laser // Nat. Photonics 4, 636–640, 2010.

[16] *M. Ravaro, C. Manquest, C. Sirtori, S. Barbieri, G. Santarelli, K. Blary, J. F. Lampin, S. P. Khanna, and E. H. Linfield //* Phase-locking of a 2.5 THz quantum cascade laser to a frequency comb using a GaAs photomixer //", Opt. Lett., vol. 36, pp. 3969-3971, 2011.

[17] *D. J. Hayton, A. Khudchenko, D. G. Pavelyev, J. N. Hovenier, A. Baryshev, J. R. Gao, T. Y. Kao, Q. Hu, J. L. Reno, and V. Vaks //* Phase-locking of a 3.4-THz Quantum Cascade Laser using a harmonic super-lattice mixer // Appl. Phys. Lett. 103, 051115.

[18] *A. Khudchenko, D. J. Hayton, D. G. Pavelyev, A. Baryshev, J. R. Gao, T. Y. Kao, Q. Hu, J. L. Reno, V. Vaks* // Phase locking a 4.7 THz Quantum Cascade Laser using a Super-lattice Diode as Harmonic Mixer // conf. proc. IRMMW-THz, 2014.

[19] *A. Danilov, N. Erickson, A. Light, and J. Waldman, // Phase locking of 2.324 and 2.959 terahertz quantum cascade lasers using a Schottky diode harmonic mixer //* Opt. Lett., vol. 40, pp. 5090–5092, 2015.

[20] *B.T. Bulcha, J.L. Hesler, A. Valavanis, V. Drakinskiy, J. Stake, R. Dong, J.X. Zhu, P. Dean, L.H. Li, A.G. Davies, E.H. Linfield, N.S. Barke. // Phase locking of a 2.5 THz Quantum Cascade Laser to a microwave reference using THz Schottky mixer* // conf. proc., IRMMW-THz, 2015.

[21] *J. R. Freeman, L. Ponnampalam, H. Shams, R. A. Mohandas, C. C. Renaud, P. Dean, L. Li, A. G. Davies, A. J. Seeds, and E. H. Linfield* // Injection locking of a terahertz quantum cascade laser to a telecommunications wavelength frequency comb // Optica, Vol. 4, No.9, pp. 1059-1064, 201

Characterization of the THz quantum cascade laser using fast superconducting hot electron bolometer

Yu. V. Lobanov[1,2], Yu. B. Vakhtomin[1,2], I. V. Pentin[1,2], R. A. Khabibullin[3], N. V. Shchavruk[3], K. V. Smirnov[1,2,4]

[1]LLC "Superconducting Nanotechnology" (SCONTEL), Moscow, Russia, lobanov@scontel.ru
[2] Moscow State Pedagogical University, Moscow, Russia
[3] V.G. Mokerov Institute of Ultra High Frequency Semiconductor Electronics of RAS, Moscow, Russia
[4]National Research University Higher School of Economics, Moscow Institute of Electronics and Mathematics, Moscow, Russia

Invention and demonstration of solid-state terahertz-range quantum cascade lasers (THz QCLs), followed by inevitable development of the fabrication technology, brought in a new era for the terahertz-range related fundamental and practical applications, such as spectroscopy and astrophysics, imaging and communication. With increase of the THz QCL research papers (with details found elsewhere, e.g., [1-4]), optimization of the lasing characteristics, improvement of its performance and development of the laser characterization techniques attracts a special attention among the researchers. There is a wide variety of different techniques for the detection of THz QCL. However, most of them are based on incoherent thermal detection with the slow time-constant of thermal process ~ 1 ms. In this paper, we present a new characterization method of THz QCL operated in the pulsed mode. In the proposed method the THz QCL is biased by applying a smooth gradual (i.e., with a "slow-rising" front edge) voltage pulse, and the laser output power was measured using NbN superconducting hot electron bolometer (HEB) within a single voltage pulse front edge, which was possible due to sufficiently short response time (of the order of 1 ns) of the HEB. The HEB which we used was similar to that described elsewhere [5]. The primary advantage of this method over the most common THz detection techniques derives from its ability to measure THz QCL output power-current relationship within a single voltage pulse. In addition, the use of a smooth gradual voltage pulse makes it possible to avoid strong fluctuations of the current flowing through the THz QCL at the beginning and the end of the driving pulse in the case of using a driving pulse with sharp edges [6]. In our setup, THz QCL was mounted onto a cold plate of a closed-cycle refrigerator, whose base temperature was varied in a range of 5 – 60 K. Principally, a very short measurement time set by duration of the driving pulse and its repetition rate (~ 5 μs and 200 Hz, respectively), prevents the QCL from overheating by the driving current. Amplitude of the driving pulse was chosen to be slightly higher than the laser threshold voltage. Fig. 1 depicts a driving pulse along with the measured lasing power which is given in arbitrary units. THz radiation was focused by a couple of off-axis parabolic mirrors onto the detector block. HEB was installed onto a cold plate of a wet helium cryostat. DC voltage and a resistive heater were used to bias the HEB to its optimal bias point where a high responsivity is obtained. THz QCL power incident on the detector was kept within detector's dynamic range. The HEB signal was amplified using a low noise cold amplifier and an R&S oscilloscope was used for the signal analysis.

THz QCL based on four tunnel-coupled quantum wells GaAs/$Al_{0.15}Ga_{0.85}As$ with a resonance-phonon depopulation scheme emitting near 2.3 THz was investigated by the proposed method. The laser was processed into a double metal waveguide based on Au with dimensions 1 mm × 100 μm ×10 μm using the conventional technology described in [7]. The laser is die bonded to a copper submount with wire bonding to ridge structures. No coatings or lens were deposited on the laser facet. A THz QCL emits radiation when the value of voltage exceeds the laser threshold level (i.e. when the laser gain coefficient is exactly balanced by the sum of waveguide and mirror losses). Applying a smooth gradual voltage pulse it becomes possible to smoothly approach the threshold condition which was examined at different operating temperatures of the QCL. As deduced from data given in Fig. 1, the laser threshold and peak power are achieved at voltages of 10.7 V and 10.8 V at 5 K, respectively. A further increase in the laser voltage is accompanied by a sharp drop in the optical power until lasing ceases at 11.3 V. After a sharp increase in output power beyond the laser threshold,

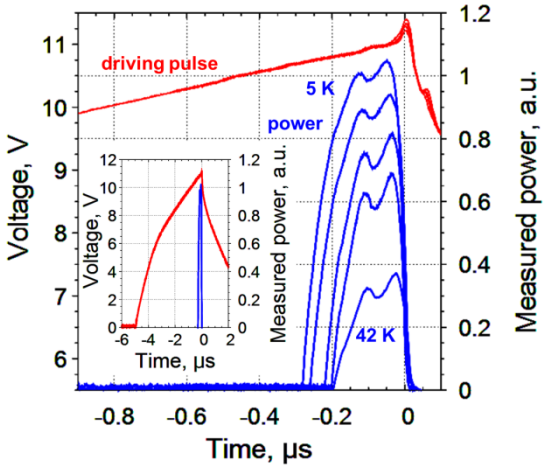

Fig. 1. QCL driving voltage pulse and measured lasing power registered with HEB. With increase of the QCL operating temperature from 5 to 60 K lasing power has decreased. In the figure, measured power at 5, 14, 36, 41, and 42 K is shown. The lasing pulse width has also decreased from ~ 250 ns at 5 K down to ~ 100 ns at 56 K. Inset shows rise and decay of the voltage pulse and relative position of the emitted THz pulse during the driving pulse

a nonmonotonic behavior of the output power-current dependence is observed. We suppose that this is due to the mode hopping effect with an increase of applied electric field. Commonly, the gain maximum shifts to higher frequencies with an increase in applied electric field, which is related to transformation of the laser levels positions [8]. The influence of temperature on the laser parameters is one of the most important characteristic of THz QCL. The temperature dependence of the threshold current J_{th} was measured by the proposed method. Using a phenomenological relationship for the temperature dependence:

$$J_{th} = J_1 + e^{T/T_0}, \quad (1)$$

we determined the characteristic temperature T_0 to be ~ 26 K. Since in our experiment we have measured rather voltage, the current was obtained using a mathematically derived fitting parameter AR such that $J_{th} = V_{th}/AR$, with $AR = 0.0217$. $J_{th}(T)$ and its fit according to (1) are depicted in Fig. 2. Following a paper by Albo & Hu [9] we have also examined $P(T)$ dependence of the QCL power and experimental results are shown in Fig. 3. The presence of second plateaus in $P(T)$ in the temperature range from 43 to 52 K is not traditional for this characteristic.

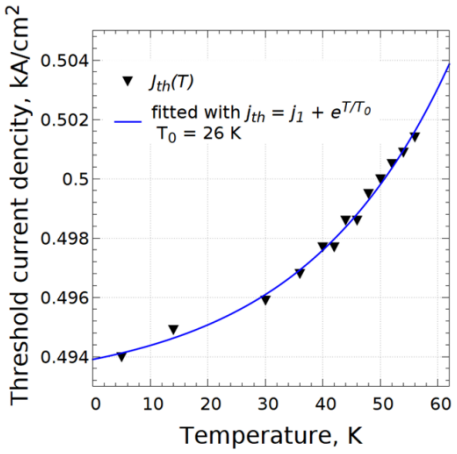

Fig. 2. Threshold current dependence on the QCL operating temperature. Experimental points are fitted according to (1)

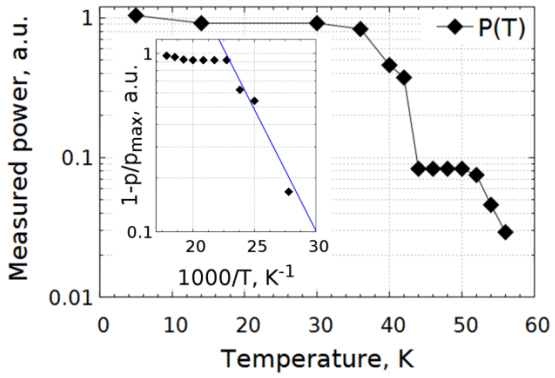

Fig. 3. Dependence of the laser output power (normalized) on the QCL operating temperature. Inset shows the Arrhenius plot with a fitting line in the temperature range 30-42 K, from which an activation energy E_a of ~ 26 meV has been derived using (2)

Typically $P(T)$ gradually decreases with increasing temperature and at high temperatures the dominant mechanism of scattering is thermally activated LO-phonon scattering [9]. The formation of the second plateau in $P(T)$ is most likely caused by the leakage of electrons from lower laser level to the continuum. Thus, a partial compensation of "negative" thermally activated LO-phonon scattering and "positive" leakage of electrons from lower laser level is obtained. Nevertheless, Arrhenius plot of the $P(T)$ dependence (inset in Fig. 3) is well fitted to:

$$\frac{P_{out}(T)}{P_{out}^{max}} = 1 - \alpha e^{-E_a/kT} \quad (2)$$

in the 30-42 K temperature range, providing an activation energy E_a of ~ 26 meV which is reasonably close to a calculated value of ~ 28 meV.

In conclusion, we have proposed and demonstrated a new approach for THz-QCL characterization allowing $P(V_{bias})$, $P(T)$, and $I_{th}(T)$ analysis. Obtained results are in a reasonable agreement with previous results; however, further study of these dependencies may reveal additional information regarding the QCL structure. Exploiting fast response of our detector and tunability of the implemented pulsed gradual biasing a thorough investigation of the QCL emittance depending on the driving parameters could be carried out.

This research has been partially supported by the RSF grant No. 17-72-30036 (development and implementation of the experimental technique, data analysis) and RFBR grant No. 17-02-00070 A (design and processing of the QCL chip, data analysis).

References

1. *Williams, B. S.* Terahertz quantum-cascade lasers // Nat. Photonics 2007. V. 1. P. 517-525.

2. *Scalari, G., et al.,* THz and sub-THz quantum cascade lasers // Laser & Photon. Rev. 2009. V. 3, No. 1–2. P. 45–66.

3. *Sirtori, C., et al.,* Wave engineering with THz quantum cascade lasers Nat. Photonics 2013. V. 7. P. 691–701.

4. *Liang, G., et al.,* Recent Developments of Terahertz Quantum Cascade Lasers // IEEE J. Sel. Top. Quant. 2017. V. 23, Iss. 4. P 1-18.

5. *Seliverstov, S., et al.,* Fast and sensitive terahertz direct detector based on superconducting antenna-coupled hot electron bolometer // IEEE Trans. on Appl. Supercond. 2015. V. 25, No. 3. P. 2300304-1 - 2300304 5.

6. *Scheuring, A., et al.,* Transient Analysis of THz-QCL Pulses Using NbN and YBCO Superconducting Detectors // IEEE Trans. THz Sci. Techn. 2013. V.3, No. 2. P. 172-179.

7. *Khabibullin, R. A., et al.,* Fabrication of a terahertz quantum-cascade laser with a double metal waveguide based on multilayer GaAs/AlGaAs heterostructures // Semiconductors. 2016. V. 50, No. 10. P. 1377–1382.

8. *Khabibullin, R. A., et al.,* Temperature dependences of the threshold current and output power of a quantum-cascade laser emitting at 3.3 THz // Semiconductors. 2018. V. 52, No. 11. P. 1381–1386.

9. *Albo, A., Hu, Q.* Investigating temperature degradation in THz quantum cascade lasers by examination of temperature dependence of output power // Appl. Phys. Lett. 2015. V. 106. P. 131108-1 – 131108-5.

Polymer waveguides for THz QCL radiation delivery and filtering

Nazarov Maxim[1], A. Shilov[2], Z. Margushev[3], K. Bzheumikhov[3], I. Ozheredov[4], A. Angeluts[4], A. Sotsky[2], A. Shkurinov[4]

[1]Kurchatov Institute National Research Center, Moscow, Russia, nazarovmax@mail.ru
[2]State Institution of Higher Education "A.A. Kuleshov State University", Mogilev, Republic of Belarus
[3]Institute of Computer Science and Problems of Regional Management of RAS, Nalchik, Russia
[4]Department of Physics and International Laser Center, Lomonosov Moscow State University, Russia

The development of suitable waveguides with low attenuation will allow terahertz technologies to rise to a mass applications level. In the known reviews of perspective fibers for the THz range [1,2] the necessary requirements of flexibility, single-mode regime and low attenuation are still not met simultaneously. For each case a compromise between the requested properties must be found. We demonstrate a possibility to meet all the requirements in a capillary waveguide structure in the case of the THz quantum-cascade laser (QCL) radiation delivery. The tube lattice fiber (TLF) formed by one ring of the eight identical capillaries shown in Fig.1(c) is the best compromise for THz range. The advantages of this structure over other known types of waveguides are: a simple manufacturing process, the single-mode regime, small size and flexibility [3,4]. Discrete transparent spectral bands with sharp slopes inherent to this structure in some cases became an advantage of the TLF. We present manufacturing technology and theory allowing to optimize the TLF for the delivery of the narrow band QCL radiation at f=3 THz frequency.

The authors have extensive experience in the manufacturing of photonic crystal fibers from glass. Despite the difficulties in applying this technology to polymeric materials, we use original approaches to fabricate specified geometric parameters of waveguide structures in the multi-stage "stack and draw" process. As a result, a polypropylene flexible waveguides were manufactured in different configurations (Fig.1). Transmission properties of those TLF types are compared as well in the report as the most transparent polymer materials.

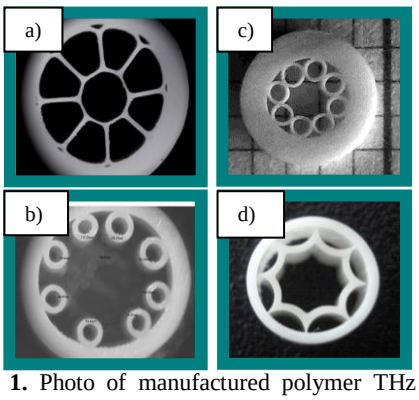

Fig. 1. Photo of manufactured polymer THz waveguides types

To create the most transparent and flexible waveguide for a fixed frequency, we studied in detail the influence of the core radius R_{core} and capillary wall thickness d (Fig.2(a)) on the shape and position of the transparency frequency windows. To characterize the fabricated TLF, it is necessary to take into account its imperfection. The wall thickness of each of the 8 capillaries in the "cladding" d_i has a random deviation of δd from the average value d. With the improvement of manufacturing technology, the size dispersion $\delta d/d \approx 0.14$ should be minimized, it is now the limiting factor to decrease d/R value and finally to decrease total TLF losses. The data in Fig.2(c) refer to polypropylene (PP) 8 capillary structure. Identical capillaries are tightly inserted into the tube cover. The ratio of the inner radius of the cover R to the outer radius of the capillaries r is given as follows: $r = R/(1+1/\sin(\pi/8))$, $R_{core} = R - 2R/(1+1/\sin(\pi/8)) = 0.4465\,\mathrm{R}$ Here R, r and R_{core} are explained on Fig. 2a). Note that number of capillaries can differ from 8.

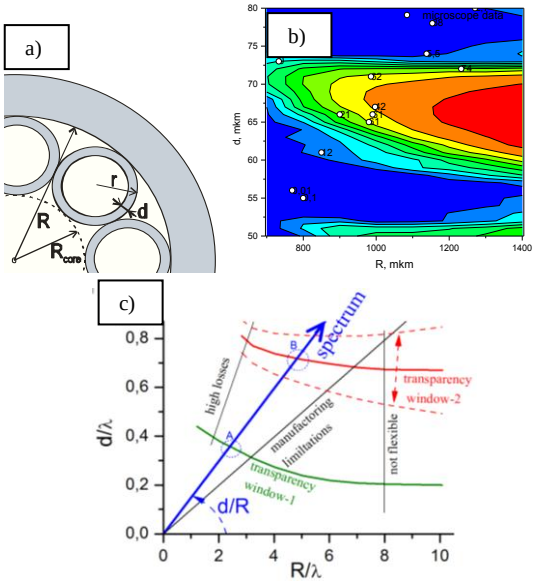

Fig. 2. a) TLF sizes, b) calculated (color area) and measured (circles) 30 cm TLF transmittance (in %) *vs* d and R, c) Optimization strategy and physical limitations for 8 capillary dielectric THz waveguide. Optimal wall thickness d *vs* air core radius R for first two transparency windows, both axes are normalized to the wavelength λ. Markers A and B indicate a particular parameters set.

The used TLF structure is optimized by two most important values - the wall thickness d (which determines the position of the transmission windows) and the core radius R, (affecting attenuation value, flexibility and modal regime). All structure proportions are given by the ratio d/R of the initial tubes, that indi-

cates how thick the wall relative to other TLF sizes is. In fact the maximum achievable transparency of TLF is determined by this ratio, it should be as low as possible till wall quality and TLF flexibility are satisfactory- Fig 2c).

Considerations for optimal *d* should account for a quasiperiodic dependence of losses *versus d*. The actual spectral position of each transparency window depends on the size of the waveguide core *R*. We choose the second transparency window as the most promising of the technically available ones. To account for the deviation from analytical estimation [4], special calculations were carried out using the methods developed in [**Error! Bookmark not defined.**]. The relationship between *R* and *d* for the center of the first and second transparency windows for a structure of 8 polypropylene (PP, n=1.5) capillaries are shown in Fig. 2c). Since polymers refraction are almost constant in THz range, for TLF analysis variation of *d* is identical to variation of $1/\lambda$, in d/λ scale we obtain universal curve (Fig. 2c), some difference appear between $R/\lambda=const$ and $d/R=const$ cases for *d* or λ variation [**Error! Bookmark not defined.**].

The measurements

To couple QCL radiation into the TLF we focused a free space radiation with a lens into a 1 mm spot on the input end – Fig. 3a). At the output end of the 30 cm long sample we measured the radiation by the Golay cell, THz camera or interferometer. For bending loss measurements we moved the output end of the waveguide together with the Golay cell.

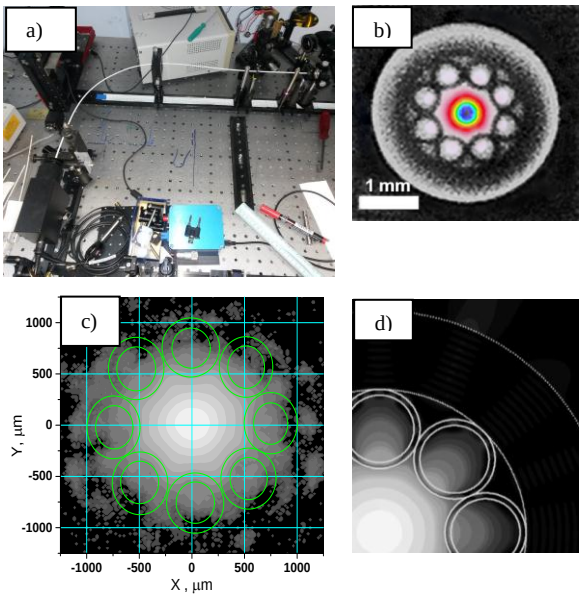

Fig.3 a) Experimental scheme photo, (b) and (c) THz field distribution of TLF mode cross-section in linear (b) and *log* (c) scales measured by THz camera. (d) Theory for fundamental mode field distribution in *log* scale.

More rigorously the shape and bandwidth of the transparency window can be measured in spectral domain by THz-TDS method for thicker walls and lower frequency – see Fig.4, for the same $\delta d/d$ and d/R average values. Using scalability of d/λ, one can compare frequency-domain spectra with wall-thickness domain spectra. The transparency window bandwidth and shape for fixed values of $\delta d/d$ and d/R are in good agreement with the theory. Note, that *d* and λ values indicated by markers *B"* in Fig.4 correspond to the second transparency window center indicated by marker *B* in Fig.2(c), in all cases $d/\lambda \approx 0.75$.

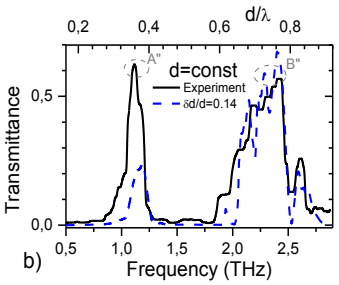

Fig. 4 Fixed *d*=95 μm and *R*=600 μm, TDS transmittance spectra - solid magenta line; dashed blue line – theory for δd/d=0.14.

In conclusion, we have demonstrated a purely dielectric, flexible, single mode, narrowband waveguide for the 3 THz frequency. In comparison with the previously known studies of TLF [5] we increased the used frequency from 0.3-1.5 THz to 3 THz, decreased the transversal TLF size from 1 cm to 3 mm. For filtering out undesirable frequencies of THz QCL radiation and selecting desired QCL frequency a set of waveguides can be used due to a steep slope of their transparency window. At the same time, the key application of the TLF seems to be a way to deliver single mode THz radiation to hardly accessible areas. A good agreement of the experimental data and theoretical calculations allows accounting for the existing technical limitations.

The work was supported by RFBR grants 18-52-00040, 17-00-00270, 16-29-11789 and BRFFI grant F18R-143.

References

1. S. Atakaramians, S. Afshar, V. T. M. Monro, D. Abbott, Adv. Opt. Photon. **5**, 169 (2013).

2. A. Bahr, B. P. Pal, G. P. Agrawal, R. K. Varshney, and M. A. Rahman, IEEE J. Sel. Topics Quantum Electron.**22**, 850015 (2016).

3. V. Setti, L. Vincetti, and A. Argyros, Opt. Express **21**, 3388 (2013).

4 M.M. Nazarov, A.V. Shilov, K. A. Bzheumikhov, Z. Ch. Margushev, V. I. Sokolov, A. B. Sotsky, and A. P. Shkurinov, IEEE Trans. THz Sci. Technol. **8**, 183 (2018).

5W. Lu, S. Lou, A. Argyros, IEEE J. of Sel.Top. In Quantum Electronics, **22**, 4401607 (2016)

Temporal stability and absolute composition issues in molecular beam epitaxy of AlGaAs/GaAs THz QCL

I. S. Vasil'evskii[1], A. N. Vinichenko[1], M. M. Grekhov[1], V. V. Saraykin[2], A. N. Klochkov[2], N. I. Kargin[1], R. A. Khabibullin[2], S. S. Pushkarev[2]

[1]National Research Nuclear University «MEPhI», Moscow, Russia, ivasilevskii@mail.ru
[2]V.G. Mokerov Institute of Ultra High Frequency Semiconductor Electronics of RAS, Moscow, Russia

The operation of the terahertz quantum cascade lasers (THz QCL) is strongly dependent on the repeatable fabrication of the well and barrier layers with the certain thicknesses throughout the whole active region stack epitaxial growth. This emphasizes the importance of the strict control of the growth rates and the stability of Si and group III effusion cell fluxes during growth [1]. It was reported [2] that two THz QCLs based on nominally identical multilayer heterostructures $Al_{0.15}Ga_{0.85}As/GaAs$ emit at the different frequencies of 2.59 and 2.75 THz because of unintentional small deviations in the GaAs and AlAs growth rates (4 and 1.6 % respectively). Authors [3] determined the thickness tolerance for working lasing heterostructures to be minimally above 2% while the structures with thickness deviation 4.3 and 6.5 % are not lasing. In [4] the Ga cell temperature has to be increased to maintain a GaAs constant growth rate while the Al cell temperature remains nearly constant because variation in AlAs growth rate can be neglected. By using such growth rate compensation technique the two nominally identical structures approximately 10 mkm overall thick were found to show thickness difference of ~ 1 %. Thus calibration procedures and accurate analysis techniques become crucial to provide enhanced metrology possibilities.

In this work we discuss the following problems which have to be solved within the QCL growth metrology: precise determination of Al content in $Al_xGa_{1-x}As$ ternary, composition profiling, robust and rapid express-analysis for AlGaAs/GaAs quantum well (QW) layer thickness and composition, cell regime corrections for proper III fluxes stabilization.

The origins of III group flow long-term drift are material rearrangement and depletion in the effusion cells and thermometry drift. The latter can arise if environmental temperature is changed and thermocouple loop hasn't reference junction.

For the absolute $Al_xGa_{1-x}As$ composition measurement the different techniques have been used: X-ray diffractometry (XRD), photoluminescence spectroscopy (PL), secondary ion mass spectroscopy (SIMS), and Rutherford ion backscattering (RBS). SIMS measurements performed in cluster ion mode with $CsMe^+$ provide good accuracy for relative composition variation. Absolute content determination by different techniques, however, gives spreading within $\Delta x \sim \pm 0.015$. Discrepancy for XRD techniques x determination arises from inaccuracy of C_{11} and especially C_{12} elastic coefficient for AlAs in the different databases. RBS are known as the most direct technique but it ensures absolute value within $\Delta x \sim \pm 0.01$ because Al haven't resolved separately but matches the area of GaAs substrate signal, so areal fit used rather than peak fit in this case. PL technique is quite sensitive [5, 6] but $E_g(x)$ dependencies have notable differences within $\Delta x \sim \pm 0.01$. PL is also can produce complicated spectrum due to doping and possible defects in $Al_xGa_{1-x}As$ (Fig. 1).

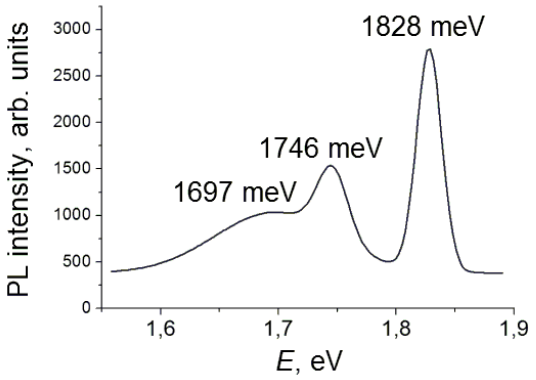

Fig. 1. PL spectra of $Al_xGa_{1-x}As$ at $T = 77$ K

Series of experiments performed on Compact 21 T epitaxy on 2 μm thick slightly Si doped $Al_xGa_{1-x}As$ (structure # 80) reveal a valuable drift of Al composition up to 1.2 %·μm^{-1} for the range of $x \sim 0.15$–0.24. After long-term cell regime stabilization and termal isolation of rear thermocouple terminals the variation has been decreased to ~ 0.1 %·μm^{-1} (Fig. 2), that could be sufficient for whole QCL structure growth.

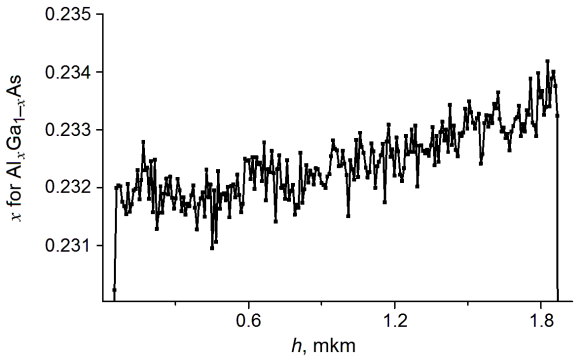

Fig. 2. Al content profile of the thick $Al_xGa_{1-x}As$ measured by SIMS

Another issue arises for superlattice structures $Al_xGa_{1-x}As/GaAs$, where both thickness and composition precision are needed. We have confirmed high efficiency of the calibration structures containing both $Al_xGa_{1-x}As$ layer and $Al_xGa_{1-x}As$ (96 Å)/GaAs (85 Å) short-period superlattice (SPSL) for the combination of metrological techniques. After proper calibration of composition and layer thicknesses, easy and fast anal-

ysis becomes possible by express technique as room temperature PL (Fig. 3). Sample # 486 has additional bulk $Al_xGa_{1-x}As$ layer that produces peak at 1.624 eV. Band structure calculation performed by Nextnano with conventional semiconductors parameters [7] shows good compliance with experiment. The technique sensitivity is about 0.6 meV energy shift per 1 Å GaAs thickness variation (Fig. 4). The absolute thickness determination accuracy for SPSL sample may be sufficiently higher by using XRD due to multiple satellite peaks and reaches 0.02 Å.

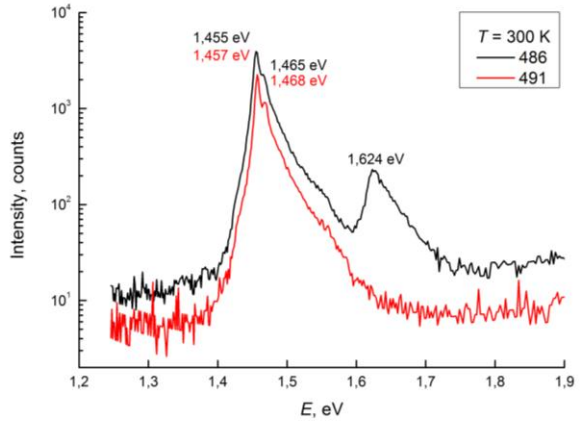

Fig. 3. Room temperature PL spectra of SPSL $Al_xGa_{1-x}As/GaAs$ samples

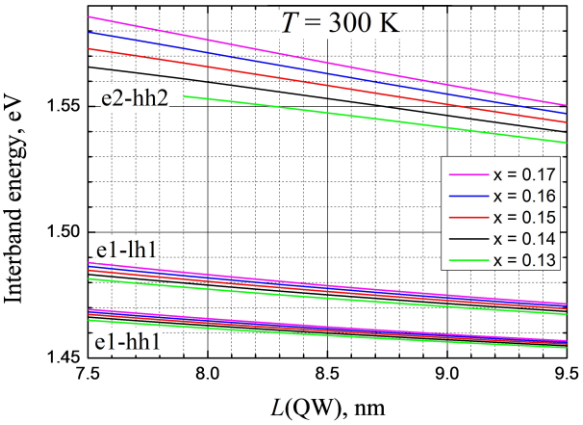

Fig. 4. Nomogramm of interband optical transitions in SPSL $Al_xGa_{1-x}As$ (96 Å)/GaAs (L_{QW})

Low temperature photoluminescence spectra of the two similar SPSL structures (samples # 486 and # 491) shown on Fig. 5 reveal excellent matching of e1-lh1 and e1-hh1 transitions in the different structures at 1.54–1.55 eV. PL measurements demonstrate high intensity of transitions and narrow well-resolved exciton peaks. The peaks beyond the quantum well energy correspond to GaAs bulk exciton (1.515 eV) and phonon replica of GaAs fundamental transition (1.473 eV). The hidden peak at 1.63–1.64 seeming as shoulder may be caused by e2-hh2 transition. Photoluminescence analysis based on e2-hh2 transition energy determination is more accurate in comparison with e1-transitions mainly in regard to *x* estimation, as one may see from Fig. 4. The explanation is that e2 energy level position is more sensitive to the height of quantum well barrier which depends on $Al_xGa_{1-x}As$ content.

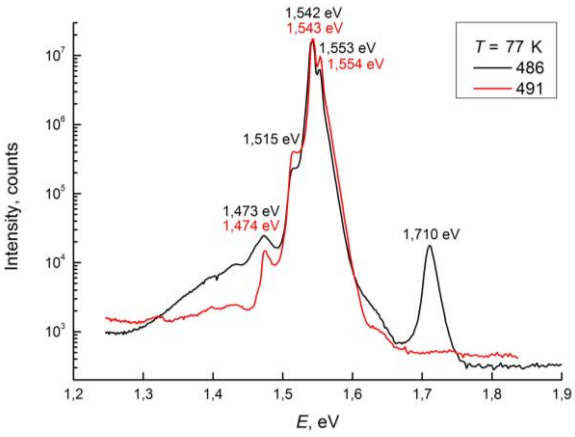

Fig. 5. Low temperature PL spectra of SPSL $Al_xGa_{1-x}As/GaAs$ samples at T = 77 K

As a result, different analysis techniques had been applied for $Al_xGa_{1-x}As$ composition analysis and spatial profile variation. XRD and PL techniques are collated and accuracy of the both are determined on short period $GaAs/Al_xGa_{1-x}As$ superlattice samples with layer arrangement, providing robust and rapid further control for QCL growth runs.

The study was partially supported by the Russian Federation President's Council on Grants (project MK-2342.2017.2) and by RFBR according to the research project № 17-02-00070 A.

References

1. *Beere, H. E., Fowler, J.,C., Alton, J., Linfield, E.,H., Ritchie, D. A., Köhler, R., Tredicucci, A., Scalari, G., Ajili, L., Faist, J., Barbieri, S.* MBE growth of terahertz quantum cascade lasers // Journal of Crystal Growth. 2005. V. 278. P. 756–764.

2. *Khanna, S. P., Chakraborty, S., Lachab, M., Hinchcliffe, N. M., Linfield, E. H., Davies, A. G.* The growth and measurement of terahertz quantum cascade lasers // Physica E. 2008. V. 40. P. 1859–1861.

3. *Roch, T., Andrews, A. M., Fasching, G., Benz, A., Schrenk, W., Unterrainer, K., Strasser, G.* High-quality MBE growth of $Al_xGa_{1-x}As$-based THz quantum cascade lasers // Central European Journal of Physics. 2007. V. 5, No. 2. P. 244–251.

4. *Li, L. H., Zhu, J. X., Chen, L., Davies, A. G., Linfield, E. H.* The MBE growth and optimization of high performance terahertz frequency quantum cascade lasers // Optics Express. 2015. V. 23, No. 3. P. 2720–2729.

5. *Galiev, G.B., Klimov, E.A., Klochkov, A.N., Lavruhin, D.V., Pushkarev, S.S., Maltsev, P.P., Vasil'evskii, I.S.* Specific features of the photoluminescence of HEMT nanoheterostructures containing a composite InAlAs/InGaAs/InAs/InGaAs/InAlAs quantum well // Semiconductors. 2015. V. 49, No. 2. P. 234–241.

6. *Lavrukhin, D. V., Khabibullin, R. A., Ponomarev, D. S., Maltsev, P. P.* Photoluminescence of heterostructures containing an $In_xGa_{1-x}As$ quantum well with a high in content at different excitation powers // Semiconductors. 2015. V. 49, No. 9. P. 1218–1221.

7. *Vurgaftman, I., Meyer, J. A., Ram-Mohan, L. A.* Band parameters for III–V compound semiconductors and their alloys // Journal of Applied Physics. 2001. V. 89, No. 11. P. 5815–5875.

3 THz quantum-cascade laser with metallic waveguide based on resonant-phonon depopulation scheme

F. I. Zubov[1], A. V. Ikonnikov[2], K. V. Maremyanin[2], S. V. Morozov[2], V. I. Gavrilenko[2], A. Yu. Pavlov[3], N. V. Shchavruk[3], R. A. Khabibulin[3], R. R. Reznik[1], G. E. Cirlin[1], A. E. Zhukov[1], A.A. Dubinov[2], Zh. I. Alferov[1]

[1]St Petersburg National Research Academic University of the Russian Academy of Sciences, St Petersburg, Russia, fedyazu@mail.ru
[2]Institute for Physics of Microstructures RAS, Nizhny Novgorod, Russia
[3]V.G. Mokerov Institute of Ultra High Frequency Semiconductor Electronics of RAS, Moscow, Russia

1. Introduction

Terahertz radiation, which frequency belongs to 0.1-10 THz range, is of great importance in various fields of science and engineering. One of the most important applications of THz radiation is the objects visualization and species detection. As this emission penetrates well through clothes and biological tissues and reflects from metals, it can be used in inspection systems for detection of hidden enclosures. At the same time, in contrast to X-ray, THz radiation is safe for living body. Promising sources of this radiation are quantum cascade lasers (QCLs), provided by their compact size, low current and voltage requirements, high brightness as well as relatively low cost. The first THz QCL was fabricated in 2002 [1]. As of today their output optical power reaches more than 200 mW in CW [2] and 1 W in pulse pumping regime [3], wavelength tuning range makes about 3 GHz for CW operation [4] and maximum lasing temperature reaches 200 K (for direct THz-emitted sources) [5]. However, QCL technology is in its infant stage in Russia.

In the present work we have fabricated and tested THz QCL having metal-metal waveguide. Heterostructure included 228 $Al_{0.15}Ga_{0.85}As$/GaAs cascades with resonant phonon based triple quantum well design. Here we present results of studies of voltage-current and light-current characteristics as well as cyclotron resonance, which allowed us to measure the lasing frequency to be about 3 THz.

2. Experiment details

Heterostructure was grown in a molecular beam epitaxy reactor (Riber 21) on a semi-insulating GaAs (100) substrate. The active region was a 228-period superlattice $Al_{0.15}Ga_{0.85}As$/GaAs. Each cascade involved three tunnel-coupled quantum wells (QW) and had resonant-phonon design. The thicknesses of the layers in the cascade in Angstroms are 43/89/24.6/81.5/41/160 (one period has 439.1 Å nominal thickness), where underlined are the dimensions of $Al_{0.15}Ga_{0.85}As$ layers. The complete width of the heterostructure was about 10 μm. Schematic band diagram at an applied bias corresponding to the lasing threshold is shown in Fig. 1a. Active transition is a transition between levels 2 and 3 with a nominal radiation frequency of 3 THz and calculated oscillator strength 0.3 at a bias field of 12 kV/cm^2. Transition 4-1 corresponds to passing of electrons between cascades (injection/extraction) and is carried out with a resonant optical phonon emission.

Growth rate was about 0.8 monolayers per second. The reactor was equipped with high speed shutters with 150 ms actuation, thus spreading of the interfaces did not exceed 0.4 Å. Layer-by-layer structure description is presented in Fig. 1b. Contact layers and the middle QW were doped with silicon concentrations of 5 x 10^{18} cm^{-3} and 5 x 10^{16} cm^{-3}, respectively. The growth was conducted in stabilized As-flow conditions; deposition temperature was controlled by IR pyrometer. The surface condition was monitored *in situ* by high-energy electron diffraction, and as grown wafer was examined by X-ray diffraction and photoluminescence technique, which spectra were compared with simulated one.

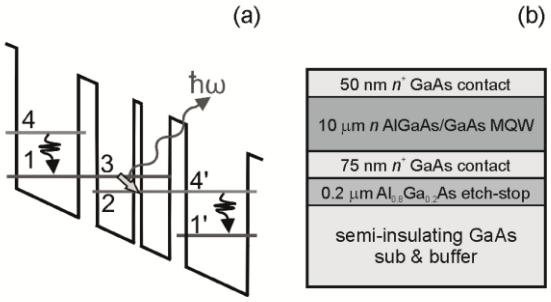

Fig. 1. (a) Schematic band diagram of QCL, (b) layer-by-layer structure description

Next metal-metal waveguide was fabricated that comprised the active region [6]. Postgrowth processing included thermal-compression bonding of the initial wafer epi-side to receptor n^+-GaAs substrate using Au-Au interlayer. QCL ridges of 100 microns width were fabricated by means of etching of the initial wafer down to the active region as well as electron lithography and dry etching of the active region through the upper metallization mask.

After thinning of the receptor to about 150 μm the wafer was cleaved to create 1.5 mm long resonators. Next chips were soldered the receptor side down to Cu heatsinks – the bottom contacts to the devices. In turn Au-wires were soldered to the ridges. The devices characteristics (voltage-current, light-current and cyclotron resonance spectra) were measured in pulse pumping regime at a liquid He temperature. To measure integral radiation intensity Ge:Ga photodetector was used. To determine QCL lasing frequency we

used variable rejecting filter based on HgTe/CdHgTe QW, which attenuation spectrum depends on magnetic field.

3. Results and discussion

Results of studies of the synthesized structure by high resolution X-ray diffractometry are shown in Fig. 2. The figure also presents calculated rocking curve. Measured superlattice period is 436 Å, differs only by 0.7% from its nominal value. Low full width at half maximum (FWHM) of satellite peaks (15-19″) indicates a high accuracy of the cascades thicknesses within the structure as well as low roughness of the interfaces. Atomic-force microscopy studies indicated the high planarity of the surface even after 10 μm growth. The widths of terraces were 0.7-1.0 μm and RMS roughness was estimated about 0.2 nm.

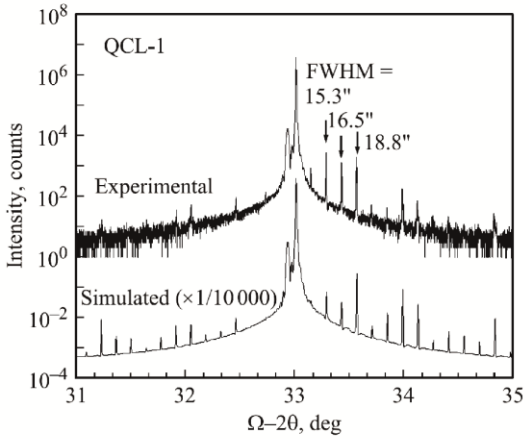

Fig. 2. X-ray rocking curve of the QCL structure near the GaAs (004) reflection and the corresponding simulated curve

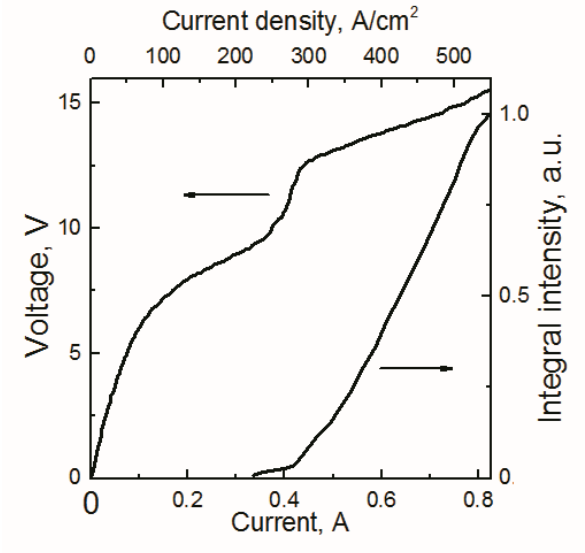

Fig. 3. Voltage-current (solid line) and light-current (dotted line) of the studied THz QCL

The dependence of the radiation intensity on the pumping current of the studied devices had characteristic threshold growth starting from 0.4 A (see Fig. 3), what is typical to the onset of laser generation. The voltage, corresponding to the kink in the light-current curve, about 11 V, is consistent with the calculated value of electric field, at which the levels are aligned, i.e. when the lasing should start (see Fig. 1a). Measurements of the radiation intensity transmitted through the variable filter based on HgTe/CdHgTe QW allowed to determine the lasing frequency of the QCL. The measured value about 3 THz coincides with the nominal frequency.

4. Conclusion

Thus, using fully domestic technological capacities we fabricated THz QCL with the double metal waveguide and the active region based on triple tunnel-coupled QWs with resonant-phonon depopulation scheme of the lower active level. High quality of the synthesized heterostructures was confirmed by high resolution X-ray diffractometry and atomic-force microscopy. Pulsed lasing was demonstrated at a liquid He temperature at 300 A/cm^2 threshold current density and 12 V voltage. The radiation frequency was estimated to be 3 THz, which is consistent with designed value.

Acknowledgements

This work was supported by the Russian Science Foundation (Project #18-19-00493).

References

1. *Köhler, R., Tredicucci, A., Beltram, F., Beere, H. E., Linfield, E. H., Giles Davies, A., Ritchie, D. A., Iotti, R. C., Rossi F.* Terahertz semiconductor-heterostructure laser // Nature. 2002. V. 417. P. 156–159.

2. *Wang, X., Shen, C., Jiang, T., Zhan, Z., Deng, Q., Li, W., Wu, W., Yang, N., Chu, W., Duan, S.* High-power terahertz quantum cascade lasers with ~0.23 W in continuous wave mode // AIP Advances. 2016. V. 6, No. 7. P. 075210.

3. *Li, H., Laffaille, P., Gacemi, D., Apfel, M., Sirtori, C., Leonardon, J., Santarelli, G., Rösch, M., Scalari, G., Beck, M., Faist, J., Hänsel, W., Holzwarth, R., Barbieri, S.* Dynamics of ultra-broadband terahertz quantum cascade lasers for comb operation // Opt. Express. 2015. V. 23, No. 26. P. 33270-33294.

4. *Hempel, M., Röben, B., Schrottke, L., Hübers, H.-W., Grahn, H. T.* Fast continuous tuning of terahertz quantum-cascade lasers by rear-facet illumination // Appl. Phys. Lett. 2016. V. 108, No. 19. P. 191106.

5. *Fathololoumi, S., Dupont, E., Chan, C. W. I., Wasilewski, Z. R., Laframboise, S. R., Ban, D., Matyas, A., Jirauschek, C., Hu, Q., Liu, H. C.* Terahertz quantum cascade lasers operating up to ~ 200 K with optimized oscillator strength and improved injection tunneling // Opt. Express. 2012. V. 20, No. 4. P. 3866-3876.

6. *Ikonnikov, A. V., Marem'yanin, K. V., Morozov, S. V., Gavrilenko, V. I., Pavlov, A. Yu., Shchavruk, N. V., Khabibullin, R. A., Reznik, R. R., Cirlin, G. E., Zubov, F. I., Zhukov, A. E., Alferov, Zh. I.* Terahertz radiation generation in multilayer quantum-cascade heterostructures // Tech. Phys. Lett. 2017 V. 43, No. 4, P. 362-365.